Numerical simulation of the development of tropical cyclones with a ten-level model. Part I

By HILDING SUNDQVIST, *Institute of Meteorology, University of Stockholm*[1]

ABSTRACT

The dynamic model is derived for an axi-symmetric vortex assuming quasi-balanced conditions. The effect of convection is included in the model through parameterization; the vertically integrated heat release is determined by the low level convergence of water vapor.

The model vertical distribution of released latent heat is based on intuitive reasoning, because of insufficient knowledge of how real cumulunimbi accomplish such processes. Qualitative discussions enable us to infer, *a priori*, how the development is affected by various *plausible* functional forms describing the heating vertically.

Two numerical experiments with different forms for the vertical distribution of heating are compared and an appreciable difference in the rate of intensification is indeed exhibited.

The results of the experiment displaying what may be considered the most realistic intensification rate, are shown in detail. A number of comparisons with empirically deduced features of the tropical cyclones indicate that the model simulates nature noticeably well.

Diagnostic studies of the energy budget of the storm reveal that the model possesses a satisfying internal consistency energetically. The rates of various energy transformations in the system compare fairly well with those estimated from observational data.

1. Introduction

The primary energy source for the development and maintenance of tropical cyclones is undoubtedly the latent heat released by condensation. Both theoretical and observational studies (e.g. Malkus & Riehl, 1960; Riehl & Malkus, 1961; Yanai, 1961*a*) show that this release takes place in tall convective clouds, "hot towers". However, the detailed mechanism for transferring the energy from the scale of cumulunimbi to the much larger cyclone scale is not yet well understood.

In the attempts by Haque (1952) and Syono (1953) to model cyclone development theoretically, the release of latent heat was directly attributed to the vertical velocity set up in the conditionally unstable atmosphere. These investigations essentially showed that, according to marginal stability conditions, cyclone scale systems would grow at a realistic rate. However, in the works by Lilly (1960) and Kuo (1961) it was shown that the above-mentioned mechanism for condensation led to systems of motion, the scales of which are characteristic for convective cells rather than for cyclone-like motions. Kuo also showed that the most rapidly growing (preferred) scale is of the same size as the cumulus scale for reasonable values of the eddy viscosity coefficient; without friction the cell would become infinitely narrow.

These conclusions were later verified in the first works on numerical models of the development of tropical cyclones, e.g. Kasahara (1961), Syono (1962) and Rosenthal (1964). The rate of heating by condensation in these models was—in the classical way—set proportional to the vertical velocity in the system. The results showed a rapid growth of the smallest possible scale of the system—an unlimited growth that made the computations blow up in a few hours.

Although the conditionally unstable stratification plays a vital role for the development of tropical cyclones, the large scale motion thus cannot be considered as a free circulation driven by bouyancy forces, but rather *a forced circulation* driven by the heat released in convective cells. And in turn, this convective activity is supplied with water vapor (and organized) by the large scale circulation—as can

[1] Contr. no. 222.

24 – 702896

be inferred from the observational fact that tremendous rainfall amounts are associated with the region of low level convergence. Hence there exists a co-operation between the two very different scales of motion and when this mutual support is sufficiently pronounced it results in a large scale self-amplification which was called *conditional instability of the second kind* by Charney & Eliassen (1964).

Thus in a model designed for studying the development of tropical cyclones, the vortex as a whole should be treated as a stably stratified system in which the condensation is a result of the vertical motion rather than the vertical motion being a result of the condensation as in convective cells. Only the collective or statistical effect of convection should be taken into account and controlled by the cyclone scale parameters. Promising results using numerical models with the cumulus convection parameterized in this way were first reported by Ooyama (1964) (although in an analysis of a linearized model). Ogura (1964) and Kuo (1965). Later, successful results were published by Ooyama (1969), Yamasaki (1968*a*, *b*) and Rosenthal (1969). Without going into the details of the different approaches to the parameterization in these works, one may say that the common idea is an assumption that the total condensational heating in a tropospheric column is proportional to the low level (1 000–900 mb, say) large scale convergence of water vapor.

In several studies on tropical cyclones, the inertial and baroclinic instability has also been discussed as important mechanisms for the formation of a tropical storm (Sawyer, 1947; Kleinschmidt, 1951; Yanai, 1961*b*, 1964; Alaka, 1963, and others). In his papers, Yanai showed that the pure inertial instability is much too weak to contribute at all to the formation. In a discussion of baroclinic instability Ooyama (1966) derived a necessary and sufficient criterion for that, in the case of frictionless flow. He concluded, however, that in order to affect the cyclone scale, the baroclinic instability should be spread over so large an area that there is no convincing observational manifestation that it would be of importance in reality. Thus, from the point of view that these types of hydrodynamic instability have a minor influence on the formation and development of tropical cyclones we may assume that the horizontal forces approximately are in gradient balance.

The objective of the present work is to construct a numerical model of the development of tropical cyclones based on the following assumptions:

(i) hydrostatic balance (p-system),
(ii) gradient balance,
(iii) axial symmetry.

From (iii) it follows that the Coriolis parameter must be constant in the vortex. The same basic assumptions were made by Ooyama (1969) in his two-layer model with a separate boundary layer. In the present model a relatively high vertical resolution is employed to make it possible to study the importance of different vertical distributions of some of the quantities, and to get a more detailed picture of the field variables during the integration.

The design of the basic model and typical results—including aspects on the energetics—from its numerical integration will be presented in this paper. A description and discussion of the numerical treatment is given as an Appendix. The evolution of a vortex as given by this model exhibits a great deal of similarity with the life cycle of tropical cyclones in nature and hence different experiments with the model should give a fairly conclusive idea of the importance of basic physical parameters (e.g. sea surface temperature, stratification) as well as of hypotheses adopted in the model. Results of such experiments are presented in a separate article (Sundqvist, 1970).

2. The governing equations of the system

2.1. *Basic equations*

According to the basic assumptions we have the following system of equations written in cylindrical coordinates for a meridional plane.

$$\frac{\partial v}{\partial t} + u\left(f + \frac{\partial v}{\partial r} + \frac{v}{r}\right) + \omega\frac{\partial v}{\partial p} = K_H\left(\nabla^2 - \frac{1}{r^2}\right)v + g\frac{\partial \tau}{\partial p} \tag{2.1}$$

$$-v\left(f + \frac{v}{r}\right) = -\frac{\partial \phi}{\partial r} \tag{2.2}$$

$$\frac{\partial \theta}{\partial t} + u\frac{\partial \theta}{\partial r} + \omega\frac{\partial \theta}{\partial p} = \frac{Q}{\pi c_p} + K_H\nabla^2\theta + \frac{g}{\pi c_p}\frac{\partial h}{\partial p} \tag{2.3}$$

$$\frac{\partial \phi}{\partial p} = -\frac{R\pi}{p}\theta \tag{2.4}$$

$$\frac{1}{r}\frac{\partial}{\partial r}(ru) + \frac{\partial \omega}{\partial p} = 0 \tag{2.5}$$

$$\frac{\partial q}{\partial t} + u\frac{\partial q}{\partial r} + \omega\frac{\partial q}{\partial p} = K_H \nabla^2 q + g\frac{\partial m}{\partial p} \tag{2.6}$$

where

$R =$ the gas constant of dry air
$c_p =$ the specific heat of air at constant pressure
$\varkappa = R/c_p$
$L =$ the latent heat of condensation
$g =$ the acceleration of gravity
$f =$ the Coriolis parameter
$v =$ the tangential wind component
$u =$ the radial wind component
$\omega =$ the vertical (p-) velocity
$\phi =$ the geopotential
$q =$ the specific humidity
$T =$ the temperature
$\pi = (p/p_0)^\varkappa$
$\theta = T/\pi =$ the potential temperature
$K_H =$ the horizontal eddy viscosity or diffusivity coefficient
$\tau =$ the tangential component of the vertical stress
$h =$ the vertical flux of sensible heat
$m =$ the vertical flux of moisture
$Q =$ non-adiabatic heating per unit mass and unit time.

$$\nabla^2 = \frac{\partial^2}{\partial r^2} + \frac{1}{r}\frac{\partial}{\partial r}$$

The first two equations are the equations of motion in the tangential and radial directions respectively; equation (2.2) is reduced to the gradient wind relation due to the basic assumption. The third equation represents the first law of thermodynamics and the fourth expression is the hydrostatic relation. The fifth equation is the continuity equation and the sixth one is the water vapor conveyance equation.

The horizontal eddy coeffient, K_H, is kept constant and has the same value for momentum, heat and moisture. The vertical flux terms are assumed to be of the following form

$$\tau = \frac{1}{g}K_v\frac{\partial v}{\partial p} \tag{2.7 a}$$

$$m = \frac{1}{g}K_v\frac{\partial q}{\partial p} \tag{2.7 b}$$

where K_v is the vertical eddy coefficient in the p-system (the approximate relation between K_v and K_z—the corresponding coefficient in the z-system—is, $K_v = (g\varrho)^2 K_z$). The vertical diffusion of heat in equation (2.3) is not taken into account in the interior of the system, because of our vague knowledge of how to discribe the vertical eddy fluxes of heat.

In the present model the non-adiabatic heating term only includes the release of heat by condensation which will be discussed in detail on section 3.

2.2 *The assumption of balanced motion*

The assumptions of hydrostatic and gradient wind balance imply that there is a direct relationship between the wind and mass, or temperature fields. This relationship is explicitly expressed by the thermal wind equation, which is obtained when the geopotential is eliminated between equations (2.2) and (2.4) by differentiating the first one with respect to p and the second one with respect to r. Thus a forecast of v and θ from one point of time to another by equations (2.1) and (2.3) shall yield new wind and temperature fields that still satisfy the thermal wind equation. In order to fulfil this requirement a certain configuration of the advecting (or meridional velocities) u and ω must exist. The equation that gives this necessary meridional circulation for maintaining the assumed balances is derived as follows.

With the aid of the continuity equation (2.5) we first introduce Stoke's stream function, ψ, in the meridional plane:

$$u = \frac{1}{r}\frac{\partial \psi}{\partial p} \tag{2.8 a}$$

$$\omega = -\frac{1}{r}\frac{\partial \psi}{\partial r} \tag{2.8 b}$$

Then we multiply equation (2.1) by $(f + 2v/r)$ and thereafter differentiate with respect to p. Furthermore we multiply equation (2.3) by $R\pi/p$ and differentiate with respect to r. Taking the local time derivative of the thermal wind equation,

$$\left(f + \frac{2v}{r}\right)\frac{\partial v}{\partial p} = -\frac{R\pi}{p}\frac{\partial \theta}{\partial r} \tag{2.9}$$

we see that the time derivatives are eliminated when the two former derived expressions are added. Thus we obtain a diagnostic equation that gives the meridional circulation when the wind and temperature fields and the non-adiabatic heating are known:

$$\frac{\partial}{\partial p}\left(\frac{A}{r}\frac{\partial \psi}{\partial p}+\frac{B}{r}\frac{\partial \psi}{\partial r}\right)+\frac{\partial}{\partial r}\left(\frac{B}{r}\frac{\partial \psi}{\partial p}+\frac{C}{r}\frac{\partial \psi}{\partial r}\right)=D \quad (2.10)$$

The quantities A, B, C and D that are functions of v, θ and Q will be given later.

From the basic assumptions it follows that it is sufficient only fo forecast v or θ, since the other can be determined diagnostically from the thermal wind equation (2.9). In order to determine the rate of heating by condensation, Q, the specific humidity also has to be forecast; this is given by equation (2.6). Then when a new set of v, θ and Q is obtained, the corresponding meridional circulation is given by equation (2.10). After that, a new forecast of v and q can be performed and so on. This is the principal idea of "quasi-balanced" prognostic systems in general; the system undergoes a continuous transition from one balanced state to another. Thus the prognostic system of the model consists of the following set of equations:

$$\frac{\partial v}{\partial t}=-u\left(f+\frac{\partial v}{\partial r}+\frac{v}{r}\right)-\omega\frac{\partial v}{\partial p}+K_H\left(\nabla^2-\frac{1}{r^2}\right)v+g\frac{\partial \tau}{\partial p} \quad (2.11)$$

$$\frac{\partial \theta}{\partial r}=-\frac{p}{R\pi}\left(f+\frac{2v}{r}\right)\frac{\partial v}{\partial p} \quad (2.12)$$

$$\frac{\partial q}{\partial t}=-u\frac{\partial q}{\partial r}-\omega\frac{\partial q}{\partial p}+K_H\nabla^2 q+g\frac{\partial m}{\partial p} \quad (2.13)$$

$$A\frac{\partial^2 \psi}{\partial p^2}+2B\frac{\partial^2 \psi}{\partial r\,\partial p}+C\frac{\partial^2 \psi}{\partial r^2}-\frac{4B}{r}\frac{\partial \psi}{\partial p}-\left(\frac{1-\varkappa}{p}B+\frac{C}{r}\right)\frac{\partial \psi}{\partial r}=r\cdot D \quad (2.14)$$

The relation between ψ and the components u and ω is given by the expressions (2.8). In the present model we have chosen to predict v, (2.11), and to evaluate θ diagnostically (2.12).

Equation (2.14) is a more elaborate form of (2.10) and the coefficients A through D are:

$$A=\left(f+\frac{2v}{r}\right)\left(f+\frac{\partial v}{\partial r}+\frac{v}{r}\right) \quad (2.15\,\mathrm{a})$$

$$B=-\left(f+\frac{2v}{r}\right)\frac{\partial v}{\partial p},\quad \left(=\frac{R\pi}{p}\frac{\partial \theta}{\partial r}\right) \quad (2.15\,\mathrm{b})$$

$$C=-\frac{R\pi}{p}\frac{\partial \theta}{\partial p} \quad (2.15\,\mathrm{c})$$

$$D=\frac{\partial}{\partial p}\left\{\left(f+\frac{2v}{r}\right)\left[K_H\left(\nabla^2-\frac{1}{r^2}\right)v+g\frac{\partial \tau}{\partial p}\right]\right\}+\frac{\varkappa}{p}\frac{\partial}{\partial r}\left\{Q+g\frac{\partial h}{\partial p}+\pi c_p K_H\nabla^2\theta\right\} \quad (2.15\,\mathrm{d})$$

The coefficient A is a measure of the inertial stability of the system, while C is the measure of the static stability and B expresses the degree of baroclinity in the vortex. The right hand member, D, that gives the forcing is a function of the distribution of momentum and heat sources.

Equation (2.14) is of the elliptic type if

$$AC-B^2>0 \quad (2.16)$$

and it has the form of a generalized Poisson equation, which together with appropriate boundary conditions determines the streamfunction uniquely. If A is negative or $|B|$ sufficiently large, equation (2.14) becomes hyperbolic. These cases imply, however, that hydrodynamic instability is present in the system; as was discussed in the introduction, this means that the balance assumptions would be inadequate. Thus, once we have accepted the balance approximation, equation (2.14) is valid only when it is elliptic. In the most intense stages in the present application we may expect $A\sim 10^{-6}$ sec^{-2} in the regions where B^2 at the same time is large; furthermore a representative value of C is 3 MTS units. Thus the ellipticity condition is still satisfied if $|B|<1.5\cdot 10^{-4}$ (MTS) which corresponds to a gradient of the order 0.5°C/km. According to analyses of the best observational material so far available (Hawkins & Rubsam, 1968*b*), it seems reasonable to expect the temperature gradient to be less than that value. Consequently we shall assume that equation (2.14) will be of the elliptic type without exception. In limited parts, A can become very small and the condition (2.16) is possibly violated; further comments on this will be made in connection with the presentation of results.

In his paper, Eliassen (1952) derived the same equation as (2.14) and discussed the general character of the solution when the forcing results from a gradient (jump) in heat or momentum, or from a point source of these quantities. We shall here briefly summarize some of the results that are of value to keep in mind for later discussions. First, from (2.15d) we see that for the forcing to appear at all, it is necessary that there is a vertical (p-) gradient in momentum and/or stress, or that there is a horizontal (along p-surfaces) gradient in heat diffusion or non-adiabatic heating. Secondly, if we focus our attention on the effect of heating, a jump in Q along a p-surface produces an upward motion on the side of the jump where Q is larger, and a downward motion on the other side of the jump. And if the meridional circulation is caused by a point source of heat, the direction of the vertical motion is upwards through the source, and downwards outside. Thirdly, a strong inertial stability (A large) or/and a weak gravitational stability (C small), gives the meridional circulation cell a large vertical and a small horizontal extension. For small A or/and large C the circulation cell becomes suppressed in the vertical and stretched out in the horizontal direction. Fourthly, the effect of baroclinity ($B \neq 0$) is to tilt the stream lines relative to the vertical axis. Thus, in our particular case with a warm core vortex, the stream lines bend outwards as we go upwards in the ascending region.

If we for the moment consider the heating in a vertical column to consist of a string of point sources (or jumps) we may conclude from the summary above that the inflow and the outflow respectively become concentrated to the bottom and the top of the column. At intermediate levels will for instance the outflow originating from a source at one level be nearly cancelled by the inflow caused by a source at a higher level. Thus if the vertical distribution of heating is such that the highest rates occur at low altitude the resulting radial motion becomes composed of a strong inflow in a shallow layer near the ground and an outflow spread over a relatively deep layer above. For the opposite distribution of heating, the inflow is spread over a deep layer and the outflow takes place in a shallow layer at high altitudes. It is hardly feasible to judge which one of the two alternative distributions converts potential energy to kinetic energy most effectively. However, the strong low level inflow gives the most effective convergence of water vapor, which then can be utilized for condensation. The more intense (and concentrated) the condensation is, the more available potential energy is created. Thus we may expect the former distribution in the given example to be the more effective one regarding intensification. This is in agreement with the quantitative results obtained by Syono & Yamasaki (1966) and Yamasaki (1968*a*).

Regarding the radial distribution of heating by condensation, we can conclude that the farther from the centre the maximum is, the farther from the centre will the maximum radial wind occur. And from absolute angular momentum considerations it is clear that the earlier (coming from the outside) the inflow ceases the less will the tangential wind be. This means that if we try to reduce the intensity or the rate of intensification by strengthening the convection artificially say, such an impulse should be given far out from the centre. The optimum distance would probably be at the periphery of the main convective region where a basic—although relatively weak—convection already exists.

2.3. *Boundary conditions*

We are going to apply our prognostic system (2.11)–(2.14) to a domain which is bounded laterally at $r = 0$ and $r = r_{\max}$. Vertically it is bounded at the ground which we approximate by $p_0 = 1\,000$ mb and at $p_T = 100$ mb which—being above the tropical tropopause—we assume to remain undisturbed.

Due to symmetry conditions we assume for the centre

$$\left.\begin{aligned} &v = 0, \quad \psi = 0 \\ &\frac{\partial \theta}{\partial r} = 0, \quad \frac{\partial q}{\partial r} = 0 \end{aligned}\right\} \quad \text{for} \quad r = 0 \tag{2.17}$$

At the top of the system we assume no-stress, zero p-velocity and constant values for both potential temperature and specific humidity.

Then

$$\left.\begin{array}{l} \tau=0, \quad \psi=0 \\ q=0, \quad \theta=\text{const.} \end{array}\right\} \quad \text{for} \quad p=p_T \qquad (2.18)$$

At the lower boundary we again assume zero p-velocity

$$\psi=0, \quad \text{for} \quad p=p_0 \qquad (2.19)$$

Furthermore we describe the fluxes of momentum, sensible heat and moisture respectively at the sea surface ($p=p_0$) in the conventional way:

$$\tau_s=\varrho C_D |V| v \qquad (2.20\,\text{a})$$

$$h_s=c_p \varrho C_D |V| (T_w-T) \qquad (2.20\,\text{b})$$

$$m_s=\varrho C_D |V| (q_w-q) \qquad (2.20\,\text{c})$$

where ϱ is the air density, C_D is the drag coefficient, $|V|$ is the absolute value of the total wind, T_w and q_w are respectively the temperature and the specific humidity of the underlying surface; thus q_w is the saturation value at temperature T_w. We shall discuss the expressions (2.20) in section 5. Considering the conditions for the outer boundary we shall first make the following remarks.

Since this study is concerned with the tropical cyclone as an isolated phenomenon, the influenced domain may be regarded as the one in which an integral balance exists between heating and cooling due to radiation. According to estimates (Malkus & Riehl, 1960; Dunn & Miller, 1964) the release of latent heat in the mature stage is about 7×10^{14} Watts. Estimated values of cooling by radiation in a tropospheric column are about 130 Watts m^{-2} (see e.g. Palmén & Newton, 1969). Consequently the cooling has to act over an area of 1 300–1 400 km radius in order to cancel the heating by condensation.

Thus choosing a computational region ($0-r_{\max}$) smaller than the above-mentioned size, the system should be treated as open.

Let us now assume B and D in (2.14) to be negligible for $r \geqslant r_{\max}$. Then treating A and C as constants the equation can easily be solved with the aid of variable separation. Requiring $\omega \to 0$ as $r \to \infty$ yields a Bessel solution

$$F(r)=E\cdot k\cdot r\cdot K_1(kr)$$

or

$$\frac{dF}{dr}=-k\frac{K_0(kr)}{K_1(kr)}F$$

Thus we have

$$\frac{\partial\psi}{\partial r}=-\frac{\psi}{L} \quad \text{for} \quad r=r_{\max} \qquad (2.21)$$

where

$$k^{-1}=\frac{p_0-p_T}{\pi}\sqrt{\frac{C}{A}}; \quad (\pi=3.14 \text{ here})$$

corresponding to the first mode in the vertical.

$$K_0(x) \quad \text{and} \quad K_1(x)$$

are the modified Bessel functions of the second kind.

and

$$L=k^{-1}\frac{K_1(kr_{\max})}{K_0(kr_{\max})}$$

For representative values of A and C, $k^{-1}\simeq 10^3$ km and then $L\simeq$ 1 800 km for $r_{\max}=600$ km, which is the value used in the numerical application. The advantage of having this special condition at the open boundary is that different sizes of the computational domain do not necessitate a reconsideration of the boundary condition itself. And it is reasonable to expect this to have a minimum influence on possible differences in the results from experiments with different $r_{\max}$'s.

The remaining boundary conditions (for v, θ, q) at $r=r_{\max}$ will be discussed and given in section 4.

3. The non-adiabatic heating, Q, and the modelling of cumulus convection

Referring to the estimates in section 2 we see that the radiative cooling will have a relatively small influence on the heat budget in a vortex of radius 600 km. Cooling due to radiation, if taken into account, should probably be applied to the cloudfree regions of the system where it affects all levels of the troposphere. The differential heating would thereby become somewhat sharpened causing a more pronounced intensification. In this first approach to a numerical model we shall, however, be content with this brief qualitative discussion concerning loss of heat through radiation. Hence, the non-adiabatic heating Q will consist solely of heat liberated by condensation. This may not only be regarded a reasonable approximation, but also a deliberate step that enables us to study the effects of the condensational heating alone, as well as to study plausible versions of the parameterization of the condensation processes.

If we knew the dynamics of individual cumulunimbi well enough, then we could—at least theoretically—of course let them be predicted by the numerical model as well, provided the resolution is sufficiently fine to describe the individual clouds properly; i.e., the horizontal mesh size should be of the order a few hundred meters. Such a fine resolution would be—even if it were practically possible—unnecessary or even undesirable in a study where the interest is focused on the dynamics of the tropical cyclone scale, which requires a mesh size of the order 10 km for a proper description.[1] We thus need to deduce a relationship that expresses the rate of condensational heating by cumulunimbi in terms of the large scale variables, (or environmental ones vis-à-vis those describing the clouds) i.e. to parameterize the convective activity.

The conditional instability of the mean tropical atmosphere is a well established fact (Jordan, 1958) and during the period July to October—the "hurricane season"—(northern hemisphere), this instability is particularly pronounced and exists through a deep layer of the troposphere. Actually, a parcel of air having its condensation level at any height below 500–600 mb on the mean sounding curve will experience buoyancy, and this is especially marked for parcels starting with surface air characteristics. An air volume following a pseudo-adiabatic ascent, starting at, or below the 900 mb level will have a free buoyancy to heights above the 200 mb surface. The "positive area" on a thermodynamic diagram, for that volume, is many times larger than for a parcel starting at or above 800 mb. Hence, we may assume that those clouds that originate from condensation in the very lowest layers will be the ones that primarily contribute to the changes of the environment. The cumulunimbi thus perform an efficient transport of heat and water vapor from low levels upwards, throughout the unstable layer, i.e. practically through the whole troposphere.

The cumulus clouds will consequently cause a gradual temperature increase—which is smaller than the one corresponding to the rate at which heat is imparted, because of adiabatic cooling through vertical motion—the upper limit being the temperature of the clouds themselves. If the environment reaches the same temperature (and the same vapor content) as the cloud has, no further temperature rise can be expected (unless a new cloud appears along a pseudo-adiabat with a higher equivalent potential temperature, θ_E). This implies that the heating by condensation is now equal to the adiabatic cooling due to upward motion. (This stage corresponds to the one where the parameter, η, in Ooyama's (1969) model becomes one. In the same paper Ooyama also shows, with the aid of a linear analysis, that for $\eta = 1$ no further intensification can be expected).

The rate of total heating by a cloud in a column is given by the flux of water vapor in through the base of the cloud in question. As was remarked in the introduction, we shall assume that this flux can be computed from the horizontal convergence of moisture below the cloud base, given by the cyclone scale parameters. Empirically we know that the radial inflow (which alone gives the horizontal convergence in an axi-symmetric vortex) in a tropical cyclone has its maximum in the boundary layer and that it decreases rapidly with height. Since the same feature also holds for the specific humidity we may conclude that the water vapor convergence in the boundary layer provides the major part of the vapor available for the creation and maintenance of clouds. The possible effects from moisture convergence above the boundary layer will be discussed later.

In view of the foregoing discussion we shall adopt the following hypotheses concerning the behaviour of the convective clouds and their influence and dependence upon the large-scale dynamics:

(*a*) Convection takes place only in regions with moisture convergence in the boundary layer; this convergence also determines the intensity as well as the horizontal distribution of the convection.

[1] If the above-mentioned possibility were a reality it should certainly be used in some investigation for the very purpose to learn how to parameterize the small scale features.

(*b*) The cloud base occurs at the condensation level of the surface air.
(*c*) We consider the penetration to be an instantaneous process in the large scale system, whose typical time scale is much larger than that of cumuli; further, the penetration is vertical and it ceases at the level where the ascent curve meets the environmental sounding.
(*d*) A cloud exists only momentarily, that is, it appears and then dissolves immediately by mixing with the surrounding air at the same level, so that the heat and water vapor brought up by the cloud are imparted to the environment.
(*e*) All condensed vapor precipitates.

3.1. *The specific formulation of the condensation model*

In order to derive the expressions for condensational heating we shall distinguish between three different conditions under which the clouds may exist. Namely,

(i) the environmental air is unsaturated;
(ii) the environmental air is saturated;
(iii) the temperature and the moisture content of the environment are the same as those of the cloud.

There will be a gradual transition from phase (i) to phase (ii) and a tendency towards stage (iii).

We first consider *phase* (*i*). According to assumptions (*c*) and (*d*) we may, at any level of the penetrated layer, put the rate of heating proportional to the temperature difference between the cloud and its surroundings:

$$Q = \xi c_p (T_c - T) \tag{3.1}$$

Similarly we have for the rate of change of humidity

$$\delta_q = \xi (q_c - q) \tag{3.2}$$

where T and q stand for the environmental (large scale) temperature and specific humidity respectively; T_c and q_c are the corresponding values of the model cloud, according to its ascent curve, where q_c is the saturation value with respecto to T_c; the inclusion of δ_q will be discussed further down; ξ is the factor of proportionality, (dimension time^{-1}), that will be determined by certain integral constraints in the following way.

The total energy input to a column on the unit area is thus according to (3.1) and (3.2)

$$\frac{1}{g}\int_{p_T}^{p_B} [Q + L\delta_q]\, dp = \frac{1}{g}\int_{p_T}^{p_B} \xi \times c_p(T_c - T) + L(q_c - q)]\, dp \tag{3.3}$$

p_B and p_T are the pressures at the bottom and the top of the cloud respectively. Consequently the equivalent amount of water vapor contributing to integral (3.3) must be equal to the available amount, which is the influx of moisture at the cloud base. The latter, C_q, is given by the following expression (from equation 2.13)

$$C_q = -\frac{1}{g}\left\{\int \frac{\partial q}{\partial t}\, dp + \int \frac{1}{r}\frac{\partial}{\partial r}(ruq)\, dp - g m_s\right\} \tag{3.4}$$

where m_s, (2.8 c), is the contribution due to the flux of vapor from the sea surface. The integral (3.4) is extended over the boundary layer. To make the basic derivation and the discussion simpler, let us first assume ξ to be independent of p. Hence, we get from (3.3) and (3.4)

$$\xi = \frac{L}{c_p} \cdot \frac{C_q}{\dfrac{1}{g}\displaystyle\int \left[T_c - T + \frac{L}{c_p}(q_c - q)\right] dp} \tag{3.5 a}$$

The quantity ξ, having the dimension of a frequency, may be interpreted as the number of times that the model cloud can appear per unit time. This number is controlled by the influx of moisture at the base and the integrated difference in equivalent temperature between the cloud and its environment.

The above derivation is principally the same as the one proposed by Kuo (1965) in his numerical model of tropical cyclone development. Kuo integrated an expression corresponding to (3.4) from the ground to the top of the cloud. It is unlikely, however, that the large scale convergence should directly support convective activity before saturation is reached, i.e. during phase (i). It rather contributes to a general moisture increase as does the term δ_q, which is added to equation (2.13) in regions of condensation during phase (i).

When *phase* (*ii*) is reached, we should extend the integration of (3.4) to the upper parts of the conditionally unstable layer in order to account for the moisture contribution to clouds starting at intermediate levels. However, the rate of vapor increase due to cumulunimbi as given by (3.2) would not be adequate during phase (ii), because when saturation is reached, this expression gives the humidity rise that would be necessary for keeping saturation, if the temperature increases further as given by the Q-term, (3.1), alone. Since there is cooling due to upward motion, the *net* heating is less than Q. Consequently, if using the expression (3.2) to compute the moisture change, we would obtain a super-saturation that rather should give rise to new clouds, otherwise too much vapor would be stored in the system and too little utilized for condensation. Thus, if we include the convergence over the whole unstable layer when computing C_q, (3.4), during phase (ii), the moisture increase in this layer should be given in proportion to the *net* temperature increase.[1] In the discussion earlier in this section it was, however, pointed out that it might be a reasonable approximation to consider only the boundary layer convergence and the clouds originating in that layer, because the major part of the water vapor converges there, and the clouds with a base below 900 mb have much higher equivalent potential temperature and thus buoyancy than those having their bases above that level. Such an assumption certainly simplifies the computations very considerably.

When phase (ii) is reached we therefore assume that all available water vapor becomes condensed and no part of it is used for raising the moisture content. This also means that we implicitly assume a sufficient, large scale convergence above the boundary layer to account for the vapor increase that is necessary to maintain saturation in spite of the possible further net increase in temperature. Consequently, the term δ_q in (3.2) drops, and the prognostic equation for the specific humidity, (2.13), loses significance in those parts of the model system. Thus we have for phase (ii):

$$\xi = \frac{L}{c_p} \cdot \frac{C_q}{\dfrac{1}{g}\displaystyle\int (T_c - T)\, dp} \tag{3.5 b}$$

[1] An attempt with a condensation model along these lines has been made by the writer. The computations blew up in a few hours however, and the impression is that some integral condition for the net temp. rise and possibly an iterative treatment is required in such a model.

For *phase* (*iii*) we may first state that Q, (3.1), will still be finite (presupposing that C_q remains finite), despite ξ (3.5 b) becomes infinite. In order to obtain Q locally in this phase we shall assume that $(T_c - T)$ becomes infinitesimal uniformly throughout the layer being considered, so that we can bring the difference outside the integral in (3.5 b). Hence using (3.1) we obtain

$$Q = L \frac{C_q(T_c - T)}{\dfrac{1}{g}\displaystyle\int (T_c - T)\, dp} \lim_{T \to T_c} = gL \frac{C_q}{(p_B - p_T)} \tag{3.6}$$

3.2. *The vertical distribution of the heating*

The importance of considering the vertical distribution of the condensational heating properly was discussed in section 2. We lack, however, observational guidance as to how this is done by the cumulunimbi. Consequently, we must resort to some hypothesis based on intuitive reasoning.

The way in which the liberated heat is distributed in the vertical by the model cloud (3.1) depends both on T_c and ξ, i.e., we must decide which ascent curve the clouds will follow as well as the vertical distribution of the frequency with which such clouds are being formed. The following two postulates may serve as a general basis for a qualitative discussion of these questions. First, the warmest possible ascent curve of a cloud is the moist adiabat through the level of the base; such a cloud consequently penetrates the greatest possible depth. Secondly, if ξ has a p-dependence, it is likely to be such that the frequency by and large decreases with height. Let us then formulate two different versions, M1 and M2, of the model condensation, regarding the vertical distribution.

M1. As a first possible approach we presume that T_c is given by the pseudo-adiabat through the cloud base and that ξ is constant with respect to p. Thus the cloud will appear equally often at the top as at the bottom of the layer being penetrated. This probably yields the most efficient transport of heat to the topmost layers of the system.

M2. A vertical variation of ξ essentially means that we try to account for the fact that a cloud may be considered to consist of several elements that start and terminate at different heights.

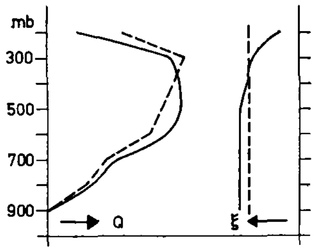

Fig. 1. The vertical distribution of condensational heating (left) and cloud frequency (*right*) owing to the two versions M1 (——) and M2 (---) of the condensation model. The environmental temperature is the one given by the mean tropical sounding.

For instance, those clouds that are initiated above 900 mb, do not reach as high up as the main cloud, and therefore tend to give ξ a maximum at some intermediate level. In the light of the discussion in section 2, we may infer that such a distribution of the heating would in comparison with M1 cause a stronger inflow at lower altitudes. Although we have regarded such clouds to be of minor influence at least energetically, they might thus have a feedback of some importance for the development. It is, however, difficult to model such features accurately, and we shall therefore use a simplified, specific approach. In the lower layers where the large scale stratification is conditionally unstable ($\partial\theta_E/\partial p > 0$) we assume ξ to be constant, while in the upper part, where $\partial\theta_E/\partial p < 0$ we let ξ decrease with height. In other words, we assume that all clouds start at the same level but only a fraction of them reach the very top because of the stable stratification aloft. Specifically we shall put ξ proportional to the difference in equivalent potential temperature ($\Delta\theta_E = \theta_{Ec} - \theta_E$) between the cloud and the surroundings in the stable layer. Denoting the level where $\partial\theta_E/\partial p = 0$ by p^* we have

$$\xi = \xi_0 \cdot n(p) \tag{3.7}$$

Thus

$$n(p) = 1 \quad \text{for} \quad p > p^* \tag{3.8a}$$

and

$$n(p) = \frac{\Delta\theta_E(p)}{\Delta\theta_E(p^*)} \quad \text{for} \quad p \leqslant p^* \tag{3.8 b}$$

We then solve for ξ_0;

$$\xi_0 = \frac{L}{c_p} \cdot \frac{C_q}{\frac{1}{g}\int n(T_c - T)\,dp} \tag{3.9}$$

As stage (iii) is approached, $n \to 1$ and hence M1 and M2 have the same characteristics in the limit as given by (3.6).

Fig. 1 shows the differences between M1 and M2 for ξ and Q if assuming the environmental temperature given by the mean sounding for the "hurricane season" according to Jordan (1958), the cloud base being at 900 mb and the air being saturated. The total amount of heat added to the column is the same in the two cases. The ξ-curve of M2 shows how the average cloud in this case "narrows" in the stably stratified region. We also notice that the maximum rate of heating in M2 is located about 150–200 mb lower down in the atmosphere compared with M1, and hence a stronger convergence of water vapor is produced by M2 than by M1. It will be shown in section 6 that this difference results in appreciable differences in the rates of intensification, with M1 giving the slower one.

Depending upon the degree of entrainment, the upward motion in the cloud will follow different ascent curves. Although this is not specifically considered in the present computation, it still seems appropriate to discuss it briefly here.

Injection of environmental air into the cloud results in a decrease of temperature with elevation, which is more rapid than the one corresponding to a moist adiabat. Hence a cloud exposed to entrainment is stopped earlier than a cloud developing as described by M1. The entrainment has thus qualitatively the same influence on the development as is described by the M2 version. Because low level convergence is enhanced in the latter case, the entrainment intensifies the large scale amplification, which is opposite to its effect on the dynamics of individual clouds. This effect should be most pronounced in the beginning of a development when the temperature difference between the pseudo-adiabat through the cloud base and the environment is large.

Admittedly, the precise formulation of the M2 version may be questioned, more so than M1, which can be regarded a strict, idealized approach. M2 is, however, related to the large scale quantities in a simple way and furthermore, in the light of the preceding discussions it may give a qualitative insight into how other conceivable processes affect the development.

Let us summarize the computational procedure in applying the condensation model.
First, the sign of C_q (3.4) is checked.
Secondly, if $C_q > 0$ and the condensation level of the surface air is in the boundary layer, ξ is computed according to (3.5a) or (3.5b), the integral being evaluated over the layer where $T_c - T \geqslant 0$.
Thirdly, Q (and δ_q where applicable) is obtained from (3.1) and (3.2) for $T_c - T \geqslant 0$.

These formulae apply to version M1. If using the M2 version, we utilize the relations (3.7) through (3.8b), and with reference to the given example (3.9) the other necessary changes are obvious. The numerical treatment of the condensation model is illustrated in section 5 and in the Appendix.

We may finally summarize the broad features of the parameterization by the following remarks. No individual convective clouds are now present in the system. They appear instead in the shape of external heat sources in a stably stratified atmosphere. The horizontal distribution and integral strength of these sources are given by the cyclone scale variables. We are here merely concerned with convective clouds when we shall settle whether heat sources are to be introduced (buoyancy) or not, and how they shall be distributed vertically.

4. Outlines of the computational treatment

In this section we only give the broad features of the computational treatment. For details and discussions of a pure numerical nature, reference is made to the Appendix.

As mentioned in the introduction, it was considered important to have a relatively high vertical resolution of the dependent variables. However, by experience we know that pronounced horizontal gradients will appear, which thus impose requirements on the resolution along the radius as well. For practical reasons (e.g., economy and reasonable execution times on a computer) we shall in most computations make the spacing between gridpoints to $\Delta p = 100$ mb and $\Delta r = 25$ km in the vertical and horizontal directions respectively. Some experiments with a finer horizontal division also ought to be run for comparison.

Bearing in mind the typical patterns that we may expect from the integrations, it would be desirable to let Δr increase with radius, thereby minimizing the computational efforts. Non-constant intervals are easily handled in an one-sided *differencing* scheme. However, in order to achieve second order accuracy for the derivatives, centered differences have been used. Consequently we keep Δr constant and hence we apply the conventional and convenient difference analogues of derivatives in a centering scheme. (In a recent paper by Sundqvist & Veronis, 1970, an efficient non-constant increment grid is proposed; however, additional investigations are required, before it can be safely employed in a prognostic system.)

The variables of the system are defined at the same grid points, except for K_v (in 2.7a, b) which is defined at intermediate pressure levels.

The diffusion terms of the prognostic equations are generally smaller than the advective ones, which thus dominate the flow. Therefore, from a physical point of view, it is reasonable to prescribe the state of the fluid only at those points of the boundary, $r = r_{max}$, where inflow takes place, while at points of outflow, the properties should be permitted to be advected out. Hence, in the present model, the following boundary treatment is adopted

$$\frac{\partial}{\partial r}(rv) = 0, \quad \frac{\partial q}{\partial r} = 0 \quad \text{for} \quad u < 0 \quad \text{at} \quad r = r_{max} \tag{4.2}$$

Furthermore, for $u > 0$ at $r = r_{max}$, v and q are obtained by an extrapolation that secures computational stability (upstream differences may be used as well). It should be emphasized that a similar treatment at the centre is also necessary for computational stability. In the present experiment, upstream differences are employed in the two point columns next the centre (see Appendix).

The potential temperature is kept constant for $r = r_{max}$ if $u < 0$. For $u > 0$, we forecast θ, noting that $\partial\theta/\partial r$ is obtained from the thermal wind relationship (2.12).

The computational scheme described in the Appendix is stable. One observes, however, an oscillation in the variables near the centre with a period of 2 Δt. Likewise, there are conspicuous irregularities in the vertical variation particularly of v. Therefore a smoothing in v is performed in the course of the integration. This smoothing is of the conventional type; i.e., a fraction of the Laplacian of the angular momentum in a point is added to the current value of $(r \cdot v)$. The shortest waves hereby become suppressed (see e.g., Wallington, 1962). In those models for numerical weather prediction where this procedure has been (or is being) used, the factor multiplying the Laplacian is usually 1/8, and the smoothing is performed every 6 or 12 hours. In the present application the factor is 1/80 and the smoothing is done every timestep. In order to be consistent with balance assumptions, the integration of the thermal wind equation, is of course carried out after the smoothing procedure on v has been applied.

5. The boundary layer treatment

In the foregoing discussions it has been inferred that the boundary layer plays a prominent role for the evolution of a tropical cyclone. Our goal will here be to take the *vertical concentration* of the inflow into account, which is of importance for the water vapor convergence. Furthermore, we shall include surface pressure (p_s) variations in order to simulate the expansion that air experiences as it moves horizontally towards the centre.

The expansion causes an adiabatic cooling that increases the temperature difference, $(T_w - T)$, with a subsequent increase in the flux (h_s) of sensible heat from the sea. The motion thus tends to be isothermal rather than adiabatic. As the pressure becomes lower, the specific humidity (q_w) of the sea surface will increase since q by definition is inversely proportional to pressure. The fluxes of moisture and sensible heat that produce a rise in the equivalent potential temperature of the inflowing surface air will thus be augmented as a result of the pressure drop along the ground.

We shall assume that the boundary layer is well mixed, implying that we will neglect vertical variations of potential temperature and moisture. Moreover, we will disregard horizontal diffusion.

The variation of the surface pressure is only taken into account in order to simulate the above mentioned processes; otherwise we will consider the boundary layer to be of constant thickness (1 000 − 900 mb).

5.1. *The drag coefficient C_D*

The description of the energy fluxes at the ground in terms of the large scale variables is a complex problem that not only concerns tropical cyclones. However, the fluxes play a decisive role in the development of a tropical cyclone, since they feature the important boundary layer. In the conventional flux expressions, (2.20 a–c), we need empirical determination of the drag coefficient, C_D. Investigations in this context, have as yet not yielded a conclusive relationship between C_D and the wind—some studies indicate a linear increase of C_D with increasing winds (Sheppard, 1958; Miller, 1963), while according to Wu (1969), C_D becomes constant for sufficiently strong winds (< 15 m/s). Consequently, the numerical values of the coefficient include some uncertainty, too. Nor is there any definite answer to the question of how well the fluxes of the different energy forms can be described by one and the same C_D. The development in Ooyama's (1969) model experiments showed a stronger dependence on differentiation of the coefficient than on the formulation of C_D, being the same for all quantities.

In view of the present uncertainties, it seems likely that a single, constant value of the drag coefficient imitates the fundamentals of the surface fluxes as confidentially as potential functional forms and differentiation of C_D would do. The former alternative is therefore adopted in this first approach to a numerical model, and an investigation of how other forms of the drag coefficient might affect the development is left for a later occasion. The drag coefficient is usually related to the wind at the "anemometer level". Here we have no such wind that is realistic however, so we are using the tangential wind at 900 mb. In the total wind, the radial component $\bar{u}$, (discussed below), is also incorporated; that is

$$|V| = \sqrt{v_{900}^2 + \bar{u}^2}$$

The numerical value of the drag coefficient is then chosen so that the resultant surface stress values agree fairly well with estimates obtained in studies of this matter in hurricanes (Palmén & Riehl, 1957; Malkus & Riehl, 1960; Hawkins & Rubsam, 1968*b*). Thus, with $\varrho = 1.2 \cdot 10^{-3}$ MTS-units, we put

$$C_D = 1.5 \cdot 10^{-3}$$

As far as it is possible to estimate beforehand, this value of C_D also yields sensible and latent heat fluxes that are in the proximity of the estimates given in the two last-mentioned references.

5.2. *The radial velocity in the boundary layer*

As already indicated through the description of the boundary conditions and of the evaluation of the right hand side of the diagnostic equation (2.14), there is formally no separate boundary layer detached when solving for ψ, as for instance in Ooyama's model (1969). With regard to the gradient balance assumption and to the present resolution (Δp = the thickness of the boundary layer) we solve (2.14) for the whole depth (1 000 – 100 mb).

The mean radial wind, $\bar{u}$, in the boundary layer is then computed from the one-sided difference analogue of expression 2.8 a; since $\psi_{1000} = 0$, we get

$$\bar{u} = -\frac{\psi_{900}}{r\Delta p} \tag{5.1}$$

The wind, $\bar{u}$, is then essentially the same as the frictional inflow that is given by the approach to a separate boundary layer (Ogura, 1964; Kuo, 1965; Ooyama, 1969).

5.3. *Water vapor in the boundary layer*

According to the approch outlined above, the q-equation (2.13) of the boundary layer consists merely of the horizontal advection and vertical eddy diffusion. In the expression for the vapor flux at the sea surface, m_s (2.20 c), q is the current moisture value in the layer, and q_w, by definition, is related to the surface pressure (p_s) as (for constant T_w):

$$q_w(p_s) = \frac{p_R}{p_s} q_w(p_R),$$

where p_R and $q_w(p_R)$ are respectively the surface pressure and q_w at $r = r_{\max}$, which are held constant. (The computation of p_s will be taken up in the next paragraph.) Since the vapor flux is proportional to the difference $(q_w - q)$, an appreciable increase may result by the pressure drop, even though the percental variation in p_s is generally small. The essential variation in p_s occurs only near the centre, why the direct energy contribution is insignificant as given by this increase, yet it permits a higher moisture content in the central parts of the vortex, thereby enhancing the differential heating, that is, the forcing of the system.

In the finite difference form, m (2.7 b) at 900 mb is evaluated analogously with τ_{800}, as described in the Appendix, A 1.

5.4. *The temperature of the boundary layer* (T_s)

In addition to the above-mentioned terms in the thermodynamic equation (2.3) we put $Q = 0$; that is, in regions with convection, the layer between the cloud base and the surface is strictly the boundary layer within which we assume $\partial\theta/\partial p = 0$.

Allowing p_s to vary, we shall rewrite equation (2.3), whereby we keep the present form of the vertical flux convergence, despite we are formally dealing with a z-system. Noticing that for instance

$$\frac{\partial T}{\partial t} = \pi\frac{\partial \theta}{\partial t} + \pi\theta\frac{\varkappa}{p}\frac{\partial p}{\partial t}$$

we thus obtain from (2.3)

$$\frac{\partial T_s}{\partial t} = -\bar{u}\frac{\partial T_s}{\partial r} + \frac{\varkappa T_s}{p_s}\left[\frac{\partial p_s}{\partial t} + \bar{u}\frac{\partial p_s}{\partial r}\right] + \frac{g}{c_p}\frac{\partial h}{\partial p} \tag{5.2}$$

In the application of equation (5.2) the horizontal pressure gradient is approximated by the gradient balance, using the 900 mb tangential wind. Integration from $r = r_{\max}$—where p as well as T are constant—to $r = 0$ yields p_s. Furthermore the pressure tendency is computed by backward differencing. Finally, the vertical eddy flux of heat at the top of the layer is omitted; consequently the last term in (5.2) is determined solely by the heat flux, h_s, at the bottom of the layer. The omission of h_{900} in cloud-free regions is probably not serious, while in those parts where convection takes place, and thus a significant upward heat flux is likely, the present approach will probably render a surface temperature that is somewhat too high in the inner parts of the vortex.

Knowing both the specific humidity and the temperature, we are able to calculate the cloud base and the appropriate pseudo-adiabat (or more generally the ascent curve) which is of great concern, as it, at each moment, determines the upper limit of the temperature in the domain of convective activity. In evaluating the integral C_q, (3.4), the boundary layer is considered to have constant thickness, $\Delta p = 100$ mb.

5.5. *The 900 mb temperature*

In order to give the vertical shear of the tangential wind or the horizontal temperature gradient at 900 mb, we need the wind, v_s, at the surface. However we cannot use a realistic value of v_s because the thermal wind relationship would then require absurd temperature gradients. So instead we resort to the potential temperature gradient as obtained from (5.2) and the p_s-distribution. We assume this gradient to be representative for the 950 mb level and then compute the 900 mb gradient by linear interpolation between 800 and 950 mb. Hence we get

$$\left(\frac{\partial\theta}{\partial r}\right)_{900} = \frac{1}{3}\left[\left(\frac{\partial\theta}{\partial r}\right)_{800} + 2\left(\frac{\partial\theta}{\partial r}\right)_{950}\right] \qquad (5.3)$$

Equations (2.9) and (5.3) then give a v_s that is consistent with the basic balance assumptions.

6. Results of a numericl integration

The main purpose of the examination of the results from one integration of the model is of course to obtain a manifestation of the capability of the model. We shall hence make a number of comparisons between the results produced by the model and analyzed observational material from real tropical cyclones.

Nevertheless, we shall start the presentation by a comparison between two model experiments; one using the M1 version of the condensation model and another using the M2 version. We shall briefly discuss the differences in the obtained results, partly in order to justify why the results of the M2 model are chosen for the detailed presentation. It should be remembered, however, that the comparison also gives interesting information concerning the physics and the modelling of the system.

First of all we shall define the initial state of the integration.

6.1. *Parameters and initial state*

The present numerical integration of the above-described model is started from a barotropic vortex where the tangential wind is the following function of the radius.

$$v = v_0\frac{r}{r_0}\exp\left[\frac{1}{2} - \frac{1}{2}\left(\frac{r}{r_0}\right)^2\right] \qquad (6.1)$$

where v_0 is the maximum wind which is located at $r = r_0$.

The eddy viscosity coefficient K_v is assumed to decrease with height in such way that, converted to the z-system, it renders K_z a linear decrease with z. At 950 mb $K_v = 10^{-3}$ MTS-units, corresponding to $K_z = 10$ m²/s, and at 50 mb $K_v = 0$.

The numerical values of the parameters are listed below:

$g = 9.8$ ms^{-2}

$f = 5 \cdot 10^{-5}$ s^{-1}, (lat. 20° N)

$r_{\max} = 600$ km

$p_s(r_{\max}) = 1\,010$ mb

$T_W = 27.5$ °C

$T_s(r_{\max}) = 27.5$°C

$q_w(r_{\max}) = 23.6$ g/kg

$C_D = 1.5 \cdot 10^{-3}$

$K_H = 5 \cdot 10^3$ m^{2}s^{-1}

$v_0 = 15$ ms^{-1}

$r_0 = 200$ km

Furthermore we have

$\Delta p = 10$ mb; $\Delta r = 25$ km

The data for "hurricane season" deduced by Jordan (1958) were used for the initial temperature and humidity distributions. Above 600 mb, however, the relative humidity was assumed to be 50%.

The choice of the initial vortex is of course to some degree arbitrary, since it is difficult to judge what should be the most realistic initial state. A relatively large value of r_0 is chosen so that it will be possible to observe clearly a diminishing of the radius of the maximum wind during the development. Furthermore, the large r_0 gives a moderate value to the relative vorticity, despite the relatively high v_0-value, which is chosen in order to reduce the computation time.

The variable time increment, (described in Appendix) was 45 minutes at the start and it decreased to 229 seconds around the time of peak intensity, and at the end of the integration (210^h) the time step was 413 seconds. The total number of steps was 2 193, and the required CPU-time on an IBM 360/75 computer was 53.4 minutes.

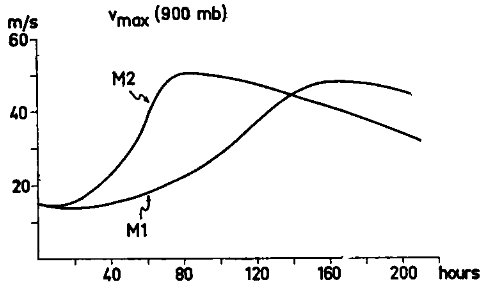

Fig. 2. Maximum tangential velocity as a function of time for the two versions M1 and M2 of the condensation model.

6.2. *Evolutionary differences obtained from the versions M1 and M2 of the condensation model*

As mentioned above, we shall first briefly compare the differences in development between the two versions M1 and M2 of the condensation model, described in section 3.

The maximum tangential wind and its variation with time is an apparent measure of the intensity and a convenient visualization of the gross characteristics of the development. In this comparison we shall look at the differences only in terms of the intensity as a function of time.

Fig. 2 shows the development of the maximum tangential wind—which occurs at 900 mb—for the two cases M1 and M2. Both versions yield an intensification of the vortex to a peak intensity whereafter the max wind slowly declines. Yet there is a significant difference in the rate of intensification. The seemingly slight difference in the vertical distribution of heating between M1 and M2 hence causes substantially different developments.

Initially, the vertical distribution of Q, as given by M1 or M2, is the same as that shown in Fig. 1. The heat that is given off to the lower half (below 550 mb) of the troposphere is then about 30 and 34% of the total heat in M1 and M2 respectively. These figures compare very closely with the corresponding initial values (the parameter l) in two of the experiments described in Yamasaki's paper (1968a). The resulting differences during the first stages of the development in his experiments are much alike those shown in Fig. 2.

With regard to the mean rate of intensification as well as to a shorter period of rapid intensification, the results produced by the M2 version seem more realistic than those given by M1. Certainly it is often observed that the intensity increases very slowly in the beginning, but usually the final intensification to a mature stage takes place over a relatively short period (of the order 10–30 hours). Therefore, the more detailed presentation of the results will be concerned with the development using the M2 condensation model.

We summarize this brief comparison by stating that the evolution is quite sensitive to the vertical distribution of the condensationl heating. Although we are able to simulate the typical development of a storm, we need a better knowledge and understanding of the dynamics of individual convective clouds in order to ascertain a correct formulation of the vertical apportionment of the heating due to condensation, in terms of the large scale variables.

6.3. *Results of integration employing the M2 version of the condensation model*

With reference to Fig. 2 we see that the maximum wind increases to 51 m/s in about three and a half days (84 hours) in spite of a decreasing tendency at the beginning of the integration. The time variation of the central surface pressure, Fig. 3, exhibits roughly a mirror image of the v_{max}-curve. The minimum pressure occurs, however, around 92 hours when it is 951 mb, or 52 mb lower than the initial value.

Fig. 4 shows how the radius of v_{max} decreases from 200 km to 50–55 km at 64 hours. Thereafter a slight increase can be discerned. Likewise, the radius of the maximum vertical velocity at 900 mb diminishes with time until approximately 72 hours when w_{max} is situated about 60 km from the centre. After 72 hours

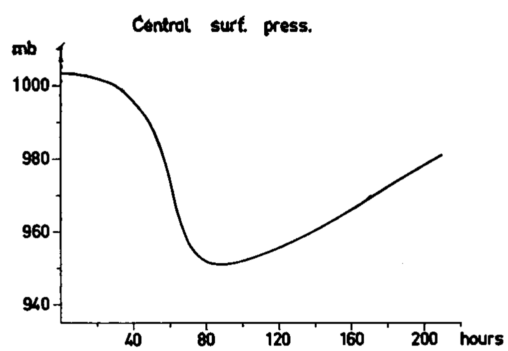

Fig. 3. The variation of the surface pressure at the centre with time.

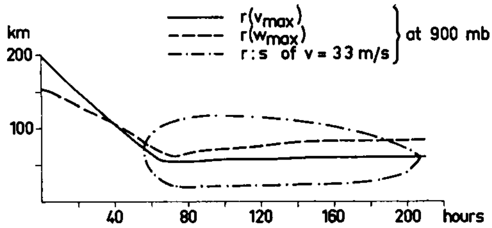

Fig. 4. Time changes of the radii of the maximum tangential velocity and the maximum vertical velocity. Within the dash-dot line, the 900 mb wind is greater than 33 m/s (hurricane force).

this curve shows a clear tendency for w_{max} to move away from the centre. In addition, it should be pointed out that this curve practically coincides with the one giving the radius of the maximum rate of precipitation versus time. Furthermore, Fig. 4 shows that hurricane force winds last for 4 to 5 days in a ring of a considerable width (50–75 km).

From this survey of the gross features of the development of the model tropical cyclone we perceive that we may divide the evolution into three or four stages like one usually does for tropical cyclones in nature.

First there is a *stage of formation* or organization; in this case, during the first 20–30 hours. The duration of this period, as well as details of the transition process, are naturally products of the initial state and the basic characteristics of the model. The gross appearance resembles however, the one observed in nature; i.e., little change in the maximum wind and a slow pressure drop at the centre. In agreement with these circumstances we observe (Fig. 4) a decrease in the radius of the maximum wind and subsequent concentration of the condensational heating (w_{max}-curve), which intensifies

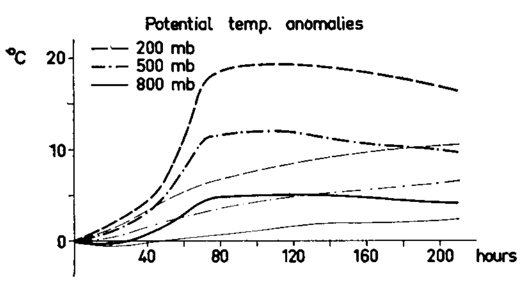

Fig. 5. Time variations of potential temperature anomalies from "hurricane season" temperatures. The anomalies are given for three different heights 200, 500, 800 mb at the centre (thick lines) and at $r = 100$ km (thin lines.)

the differential heating, i.e., the forcing of the system. Furthermore a net warming takes place essentially in the upper half of the troposphere during this stage. This is seen in Fig. 5, which displays the variation of the potential temperature anomalies at the centre and at 100 km for three different heights. In fair agreement with the reports from several case studies (e.g. Yanai, 1961*a*; Zipser, 1964; Hawkins & Rubsam, 1968*a*) we observe a transition to a warm core, beginning at high altitudes. The conversion of potential to kinetic energy is thus made easier. The stabilization in the upper part also has the important effect to shift the maximum heating downwards and thereby causing an increased inflow in the lowest layer of the system.

Secondly, there is a *stage of pronounced intensification*. The model vortex undergoes a rapid change of state during a time period that compares well with observations of real cyclones. The average rate of pressure fall (30^h–84^h), for instance, is about 20 mb/d, but there is also a period from 50^h to 70^h when the pressure drops 32 mb (Fig. 3). These figures accord closely with the corresponding ones given in the papers by, e.g., Colon & Staff (1961), Yanai (1961*a*) and Hawkins & Rubsam (1968*a*). Fig. 5 shows that the final transformation to a distinct warm core vortex proceeds very rapidly, while the further concentration of winds and precipitation takes place with the same pace as during stage one (Fig. 4).

Thirdly, there is a *mature stage*, which begins between 70 and 80 hours in the present experiment. In this period, an abrupt decline in the rate of change of the vortex comes about. The final approach to minimum central surface pressure (Fig. 3) and maximum temperature anomalies at the centre (Fig. 5) proceeds very slowly. The radius of maximum rate of precipitation exhibits a clear tendency to increase immediately after the minimum is attained, (Fig. 4). Since this effect implies that the differential heating is changing continuously, we cannot expect to find a steady state of the system. We are also led to the same conclusion by studying the variation of the temperature anomalies in Fig. 5. Although the temperature reaches a near steady state at the centre, there is a continued temperature rise farther out (100 km) throughout the integration. Thus, there is an uninterrupted increase of the size, and a decrease of the sharpness of the warm core.

The outward migration of w_{max} in the mature stage causes, by and large, a weakening of the forcing. Likewise, the decrease of the warm core intensity reduces the conversion rate of potential to kinetic energy in the system. Hence we may expect a decline of the intensity sooner or later during the mature stage. The changes are, however, so gentle that it is difficult to find a logical point where additional division of the life cycle of the model vortex should be made. Not until the cyclone is subject to external changes (landfall, pole-ward motion), may a motivation appear for a subdivision of this third phase into a mature and a *decaying stage*.

The decay of the idealized system as shown in the present integration is, of course, practically impossible to verify with the aid of real observations. This tendency is, however, a realistic dynamical feature as we have seen from the above discussion of the continuous change of state of the model vortex. The predicted rate at which the decay occurs may possibly be overestimated by the model, because of the smoothing procedure and truncation. We shall return to this matter in the survey of the energetics. (Ooyama (1969*a*) has later presented results that showed nearly steady-state in v_{max} after the mature stage was reached. The results were produced by a model with another approach to the treatment of the boundary layer; the wind in that was computed from the primitive equation of motion under a quasi-steady-state assumption.)

Let us next look at the structure of the model cyclone in more detail.

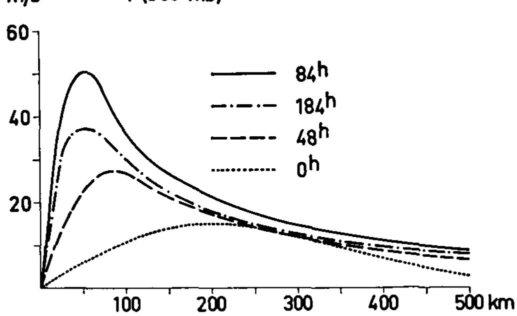

Fig. 6. Radial distribution of the 900 mb tangential velocity at 0^h, 48^h, 84^h, and 184^h.

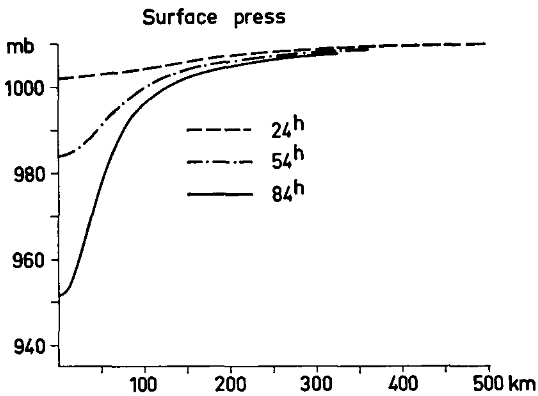

Fig. 7. Surface pressure distribution at 24^h, 54^h and 84^h.

Fig. 6 shows the radial distribution of the 900 mb tangential wind at four different times. This depicts both the concentration and the increase (and decrease) of the wind. With regard to the relatively small time changes in the wind outside 200–250 km radius, one may, from a phenomenological point of view, consider the hurricane to be a vortex with a typical diameter of 400–500 km.

It is customary to consider a functional form of the wind, outside its maximum, according to the expression,

$$v \cdot r^{\beta} = \text{const.}$$

However, only piecemeal constant values of β can be accepted for such a description of v in the present results; the exponent β increases with radius. At 84^h one obtaines $\beta = 0.77$ around $r = 100$ km, and $\beta = 0.86$ around $r = 225$ km. In the outer parts of the vortex β is very close to 1.0, with a tendency for even being slightly greater than unity. The value of β grows with time in the inner parts while it is approximately steady farther out.

Fig. 7 portrays the surface pressure, as a function of radius, at three times. It is seen that the effect of pressure variations along the surface, that was discussed in section 5, is noticeable only over a very small part of the sysem.

In Fig. 8, the radial variation of the rate of precipitation, and the vertical velocity at 800 mb, are exhibited for different times. We notice the shrinking of the convective area during the development, as well as the high

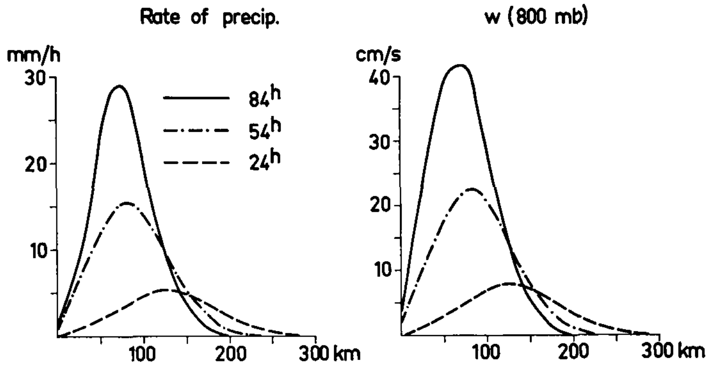

Fig. 8. Radial distribution of the rate of precipitation (*left*), and the 800 mb vertical velocity (*right*), at 24^h, 54^h and 84^h. (Outside 200–300 km radius, w is so small that the scale used is unsuitable for representing w there).

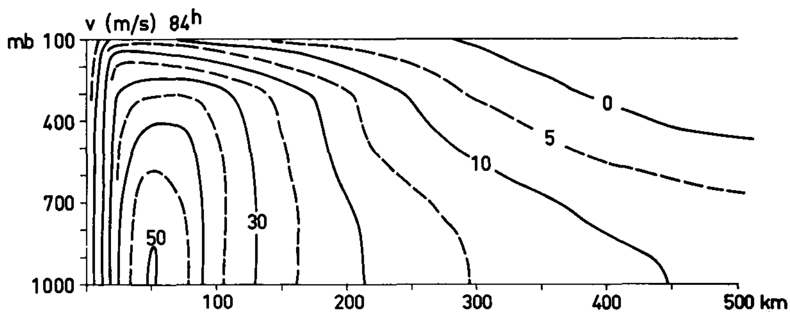

Fig. 9. Vertical cross section of the tangential velocity at 84^h.

correlation between the vertical motion and the rate of precipitation. Furthermore we observe that practically a negligible amount of rain falls at the centre; a quality that usually is assigned to the characteristics of the eye of a hurricane. Additional comments concerning the precipitation will be made in the subsection on the energetics.

Since the most complete data sets in connection with hurricane development are collected in mature storms, it is of special interest to study some of the variable fields at peak intensity (84^h) of the computed hurricane for additional comparison.

The vertical cross sections of the tangential, radial and vertical velocities are presented in Figs. 9, 10, and 11 respectively. The general distribution of v looks realistic in comparison

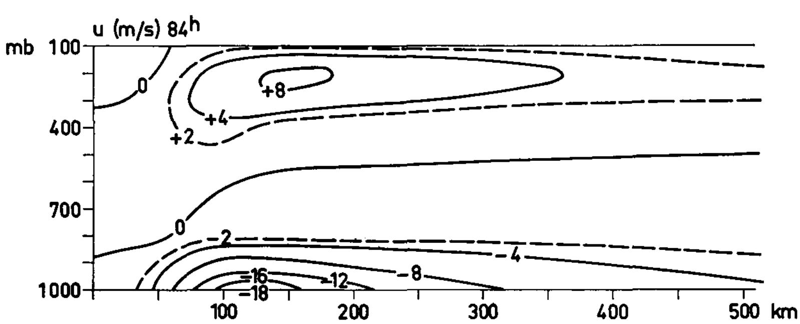

Fig. 10. Vertical cross section of the radial velocity at 84^h.

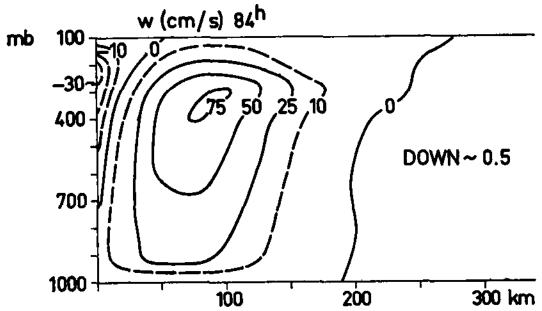

Fig. 11. Vertical cross section the vertical velocity at 84^h.

with observations (e.g. Colon & Staff, 1961; Hawkins & Rubsam, 1968*b*). Because of the relatively crude horizontal resolution, the concentration around the centre is less pronounced in the computed cyclone, than is often observed in nature. In agreement with the remark by Hawkins & Rubsam, the strong winds extend to high altitudes in the central part of the vortex.

In the zone, 175–275 km, of anticyclonic shear between 200 and 400 mb, the absolute vorticity is nearly zero or even slightly negative in some of the points. The first sign of such a feature appears at 48^h, and it is then present throughout the period of integration.

Both Rosenthal (1969) and Yamasaki (1968*a*)—who used models based on the primitive equations where hence negative absolute vorticity may appear without violating basic assumptions—state that the appearance of negative vorticity is a consequence of the development, and that there is no apparent effect on the evolution.

No anomalous behaviour, of the development or of the rate of convergence when the diagnostic equation is solved, has been detected in the present integration either. As pointed out by Ooyama (1969), the uniqueness of ψ is maintained, even if the absolute vorticity becomes negative, provided it is confined to a small region.

In the presentation of the radial velocity (Fig. 10), the boundary layer wind, $\bar{u}$, is plotted along the 1 000 mb surface. The concentration of the inflow to the lowest layers and the outflow to the uppermost layers—in accordance with empirical deductions—is clearly exhibited by the model cyclone. We also notice a weak inflow at the top, near the centre. Hence, there is a subsiding motion that does not penetrate all the way down to the ground, however, because of the opposing effect by the frictionally induced inflow there. This feature is more distinctly displayed in the vertical velocity field (Fig. 11).

In Fig. 11, we hence see what may be considered the typical quality of an eye; a region of sinking motion to rather low altitudes, causing clouds to dissolve within a small radius around the centre. This subsidence is a permanent feature, practically during the whole evolution. At the beginning it is confined to 200 and 300 mb, from where it penetrates downwards during the development, until the 700 mb level is reached around 84^h. Thereafter the tendency is reversed. At 210^h there is subsidence only down to somewhat below 400 mb. With regard to the pattern of the radial motion, it is quite plausible to expect a cirrus shield at the top, and cumuli in the low layer. This is in good agreement with for example the discussion of this matter in the book by Palmén & Newton (1969).

The magnitude of the upward vertical velocity does not look excessive. It is rather possible that a higher radial resolution would yield a more concentrated and stronger upward motion than is shown in Fig. 11.

The humidity field is not reproduced here since it can be described verbally. On the whole, it exhibits saturation in the convective region (Fig. 8 left), and a relative humidity of 40–80 %—with the lower value aloft—outside that region. However, at 200 mb, saturation prevails out to 250 à 275 km radius. Thus we may infer that a cirrus shield can extend about 100 km outside of the area of any appreciable convective activity.

It is also interesting to compare the form of the horizontal stream lines in the model hurricane, with those deduced on empirical basis (e.g. Palmén & Newton, 1969). The stream lines of the flow in the boundary layer are computed from v_{900} and $\bar{u}$.

The maximum angle of cross isobaric inflow at 84^h, thus obtained, is 33 degrees at $r = 150$ km. The resulting pattern at 84^h in the boundary layer and at 200 mb are shown in Figs. 12 and 13 respectively. The dashed circle in both Figs. marks the very outskirts of the condensation region. The radar echoes of hurricane

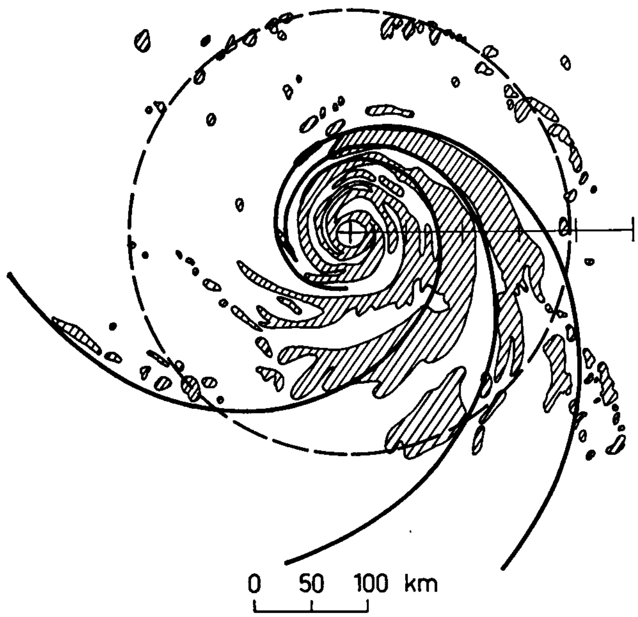

Fig. 12. Computed stream lines in the boundary layer at 84^h. Hatched areas show radar echoes of hurricane Daisy, 1958. Dashed circle marks the outer border of the computed condensation region.

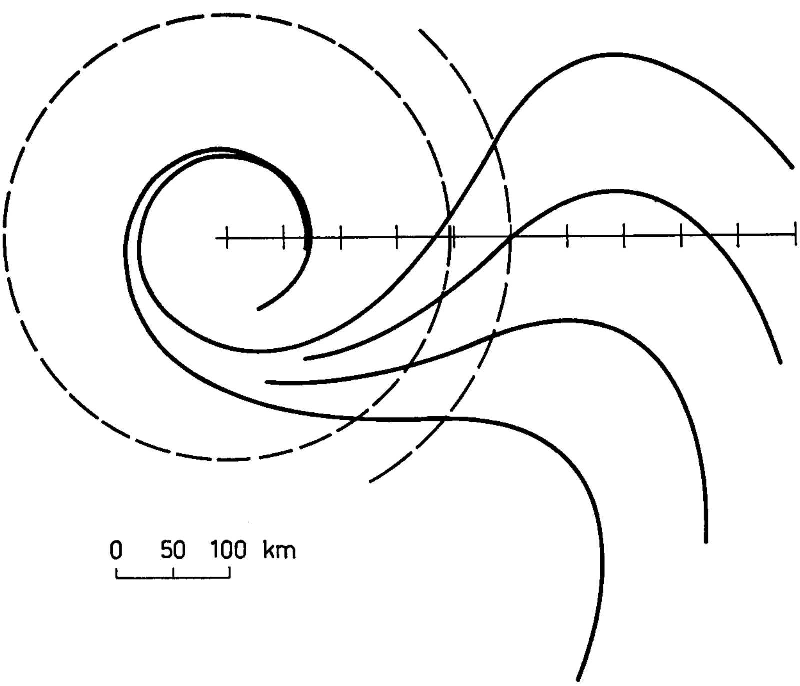

Fig. 13. Computed 200 mb stream lines at 84^h. The dashed circle is the same as in Fig. 12, and the dashed arch denotes the radius outside which subsidence prevails, and hence cirrus clouds start to dissolve.

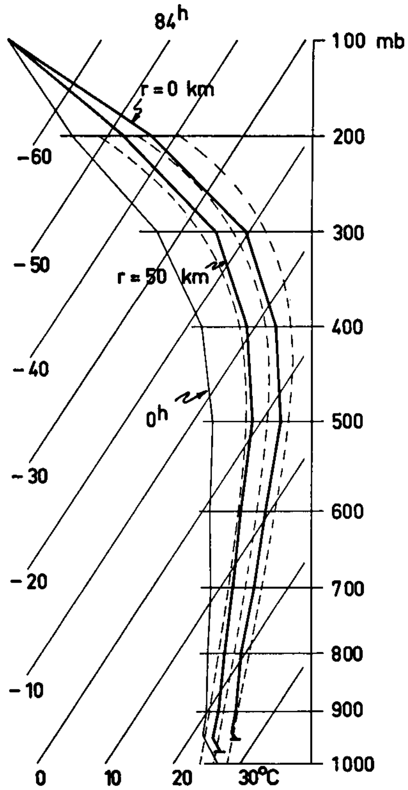

Fig. 14. The 84^h temperature soundings at the centre and at 50 km radius. The thin line shows the sounding of the initial vortex. Dashed lines denote moist-adiabats.

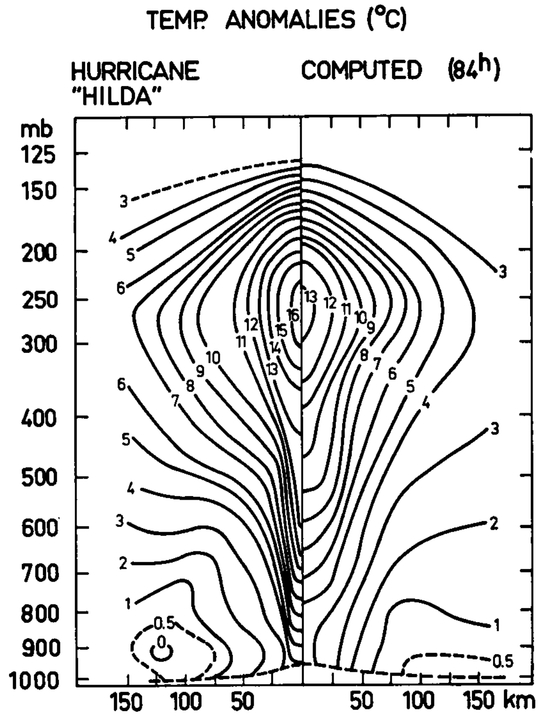

Fig. 15. Vertical cross section of temperature anomalies. The right part shows the computed anomalies (from the "hurricane season" values) at 84^h. The left part shows the anomalies (from the mean annual tropical atmosphere) of hurricane "Hilda" (west) according to the analysis by Hawkins & Rubsam (1968*b*). (The left part is a reproduction from that work.)

Daisy (1958) in Fig. 12, are shown with the mere intention to illustrate the general resemblance of the spiralling structure in rain bands, and low level winds. The dashed arch in Fig. 13 denotes the radius where one may expect that the cirrus deck starts to dissolve.

There is also a good deal of similarity between the model thermal structure, and the general characteristics of that derived from observations. The temperature soundings at 84^h for $r = 0$ and $r = 50$ km are shown, together with the sounding of the initial (barotropic) vortex, in Fig. 14. (In the layer 900–1 000 mb the sounding curve follows the moist-adiabat of θ_{900} downwards, until it intersects the dry-adiabat of the surface temperature.) We notice that the stratification has become moist-adiabatic in the area of condensation. At the centre, the absolutely stable stratification that may be considered as typical of real storms (see e.g. Hawkins & Rubsam, 1968*b*; Palmen & Newton, 1969 where also additional references are found) has not been produced by the model. Results from a preliminary experiment with a higher radial resolution indicate that this default is a consequence of the rather coarse grid along the radius. It seems reasonable to expect a more pronounced response in the temperature, particularly above 700 mb, than the present results show.

Fig. 15 depicts a composed vetical cross section of temperature anomalies. The right part displays the computed anomalies from the "hurricane season" atmosphere (Jordan, 1958). The left part shows the anomalies from the mean annual tropical atmosphere (Jordan, 1958) according to the analysis by Hawkins & Rubsam (1968*b*) (reproduced from their work). In this comparison with an individual real case, one finds of course differences in details, but

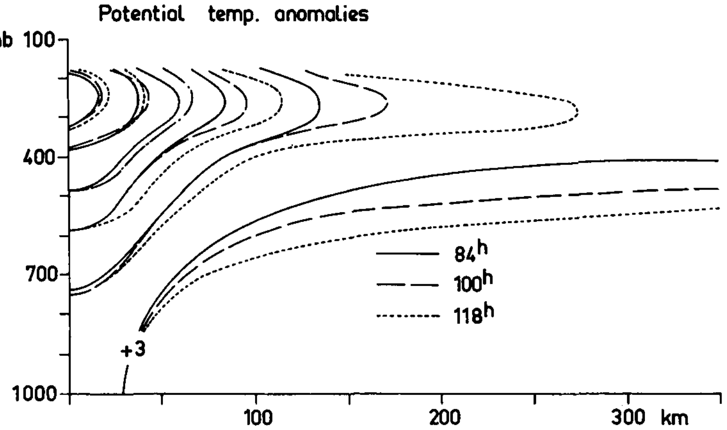

Fig. 16. Vertical cross section of potential temperature anomalies at 84^h, 100^h and 118^h. The interval between the isolines of respective case is 3°C.

the figure shows that the model produces the characteristics of the anomaly pattern well. The differences between the computed and the observed cases are again a demonstration of the default and of the numerical effects discussed in the preceding paragraph; note, for instance, that the major part of the observed temperature gradient below 400 mb lies inside the radius 25 km which corresponds to the first gridpoint in the experiment.

Fig. 16 shows the vertical cross section of potential temperature anomalies at 84^h, 100^h and 118^h. The outward transport aloft, of relatively warm air, from the central parts is clearly displayed. As the temperature near the centre is approximately constant with time, this transport thus causes a gradual degradation of the pronounced warm core and a subsequent decrease in the conversion rate of potential to kinetic energy (see e.g. Palmen & Riehl, 1957).

6.4. *Survey of the energetics*

The time variation of the total kinetic energy, (K), of the system (0–600 km) is shown in Fig. 17. By and large, this curve exhibits the same features as does the v_{max}-curve (Fig. 2), although the former one reaches its maximum 10–12 hours later. The decrease in the kinetic energy after about 100^h is qualitatively quite consistent with the spread of the warm core aloft, as discussed above. It was remarked earlier that the decrease in intensity, and hence in kinetic energy as well, is probably somewhat augmented by truncation and smoothing in the numerical procedure. On the other hand, it has also been pointed out that the smoothing suppresses much of small scale horizontal and vertical irregularities near the centre and thereby yields a more realistic appearance in the variable fields; e.g., the relatively strong winds reaching high altitudes.

An eddy diffusion that is relatively strong in the central parts and weak farther out, would give the same effect as a smoothing process. Such a diffusion can be physically motivated by ascribing it to the convective activity, (Gray, 1966). (In fact, Ooyama (1969) has a momentum transport by convective elements built into his model.) This kind of small scale, comparatively vivid exchange, is confined to a small part of the whole vortex area. The dissipative effect on the total kinetic energy would therefore probably be relatively small, compared with the one caused by the smoothing

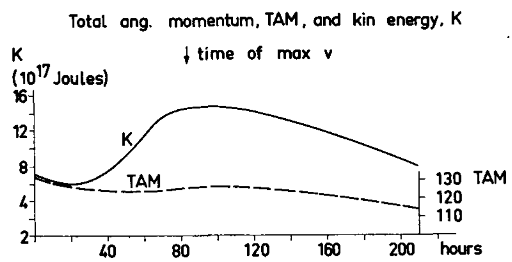

Fig. 17. Total kinetic energy, K, and total angular momentum, TAM, (0–600 km) as functions of time.

procedure. A parameterization of fluxes of different quantities due to convective processes would, however, with the present knowledge of the subject be quite arbitrary and thus uncertain.

The variation of the total absolute angular momentum, TAM, is also shown in Fig. 17. The constancy of TAM contrasts strikingly with the variation of K. From the fact that the absolute angular momentum of the cyclone shows such small a variation during the integration, we may conclude that the size of the computational domain has been chosen sufficiently large. There is of course an inward flux of angular momentum over the open boundary. This flux is nearly balanced by frictional destruction however, and hence there is, on the whole, only a redistribution of a given amount of angular momentum in the system during the evolution.

The condensational heating inside 100 km radius, as well as that inside the annulus 100–200 km radius, are portrayed in Fig. 18, in terms of an average rate of precipitation over the respective areas. We notice the increase in differential heating during the deepening stage. After about 80–84 hours a marked weakening of the forcing begins, because the heating decreases by and large only inside 100 km. This fact again demonstrates the consistency in the general behaviour of the system.

The computed average precipitation within 100 km radius agrees closely with the values obtained by Rosenthal (1969). If it is assumed that the hurricane moves with a speed of 12 km/h, then the rainfall would amount to about 35 cm at a point that is passed by the eye of the storm; if we disregard the precipitation outside 100 km, the corresponding figure would

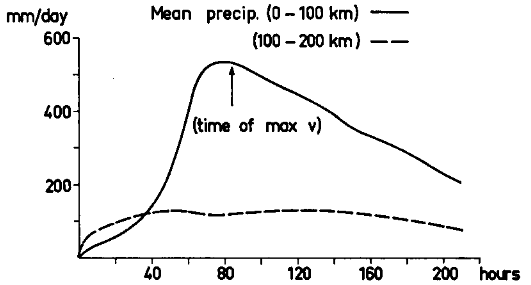

Fig. 18. The variation with time of the rate of mean precipitation (converted to mm/day) in the intervals 0–100 km (——) and 100–200 km (– – –).

be 25 cm. These values are in fair agreement with estimates based on observations (see e.g., Riehl & Malkus, 1961; Dunn & Miller, 1964; Hawkins & Rubsam, 1968*b*). With the same premises Riehl & Malkus, for instance, estimated a rainfall amount of 30 cm for hurricane Daisy on August 27, 1958.

The energy budget of the system in the course of the integration has been studied in some detail. The various terms that contribute to the energy changes have been integrated over the whole depth directly, while the horizontal integration has been carried out over different radial intervals.

A few remarks concerning the integration, or rather the summation, should be made.

In order to obtain the best possible consistency in the summation regarding the finite difference formulation of the actual prognostic equations, the advective terms have been summed up over the interval in question, $(0 - r_B)$ say. Since $\omega = 0$ at the bottom and the top of the system these sums yield the transport across the lateral boundary. In the numerical integration of v, however, the horizontal advection is computed in terms of the angular momentum derivative. So, in view of the relatively coarse resolution along r, there is a possibility of discrepancy between the transport of kinetic energy (KBT) across r_B as interpreted by the actual prognostic equation, and as it comes out from the summation; this is also the case for the rate of conversion of potential to kinetic energy (P, K). The sum from $r = 0$ to $r = r_B$ of v times the advective terms as given in (2.11), thus gives

$$KBT = -\frac{2\pi}{g}\int_0^{r_B} rdr \int \left(uv\frac{\partial v}{\partial r} + \omega v\frac{\partial v}{\partial p}\right) dp \quad (6.1)$$

and the rate of conversion of potential to kinetic energy, (P, K), is hence summed up separately as

$$(P, K) = -\frac{2\pi}{g}\int_0^{r_B} rdr \int uv\left(f + \frac{v}{r}\right) dp \quad (6.2)$$

The thermodynamic equation, (2.3), is multiplied by $c_p(p/p_0)^{\varkappa}$, in order to obtain the enthalpy changes. Then the advective terms are summed up, also here like

$$E_{AD} = -\frac{2\pi}{g} c_p \int_0^{r_B} rdr \int \left(u\frac{\partial T}{\partial r} + \omega\left(\frac{p}{p_0}\right)^{\varkappa}\frac{\partial \theta}{\partial p}\right) dp \quad (6.3)$$

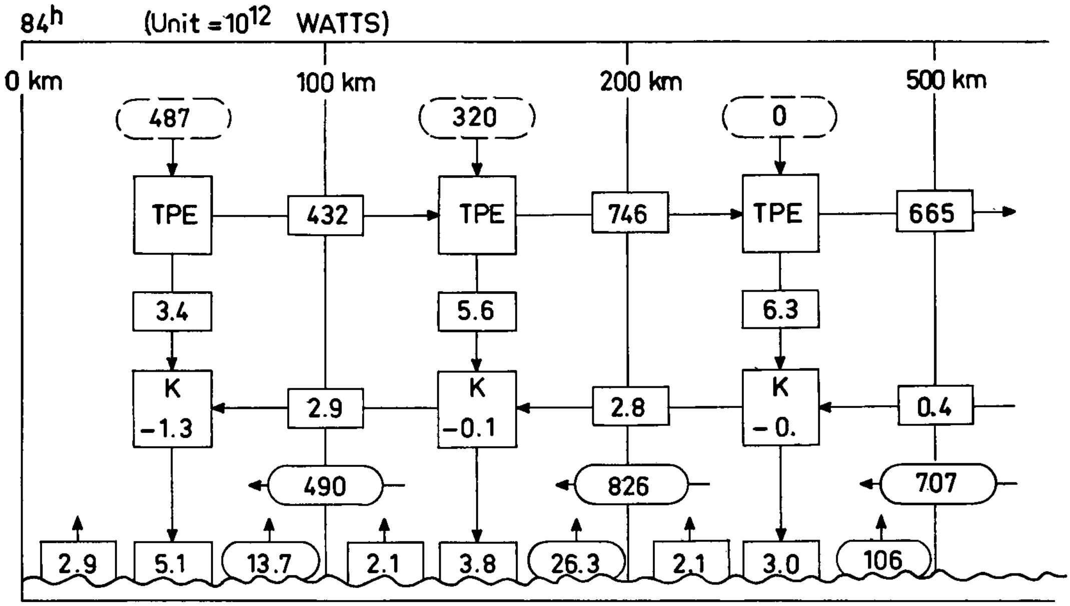

Fig. 19. Contributions to the energy changes at 84^h computed for three radial intervals. The squares *TPE* and *K* represent, respectively, the total potential energy, and the kinetic energy in each annulus. The arrows indicate the direction of the transports or the rate conversion. Ovals are used for latent energy transports, and the dashed ovals represent the energy input through condensation. The number in the *K* box shows the rate of internal dissipation. The upper rectangle on the lateral boundary represents the transport of relized energy $(c_p T + \phi)$, while the lower one gives the kinetic energy transport. The quantities transported through the sea surface are, from left to right respectively, sensible heat, kinetic energy, and latent energy. The unit is 10^{12} Watts.

(In 6.1–6.3, $\pi = 3.14$)
By some manipulation one finds that the transport of realized energy (sum of enthalpy and potential energy) at r_B, RBT, is obtained as

$$\mathrm{RBT} = E_{AD} + (P, K). \tag{6.4}$$

The evaluation of the latent energy changes is made analogously, but it is more straight forward and hence requires no further comments.

The contributions to the energy changes at 84^h, evaluated for the radial intervals (0–100 km), (100–200 km) and (200–500 km) are presented in Fig. 19. The squares TPE and K represent respectively the total potential energy and the kinetic energy in each annulus. The arrows indicate the direction of the transports or the conversion (P, K). The latent energy transports are given in the ovals; the dashed ones symbolize condensation. The upper rectangle on the lateral boundaries gives the transport of realized energy, and the lower one the transport of kinetic energy. The transport of sensible heat from the sea is given in the rectangle to the left at the bottom. The rate of internal dissipation that is given in the K box, includes in fact also the lateral eddy transport of kinetic energy. Its contribution is however small. This fact is also established from real data; see Riehl & Malkus (1961).

An algebraic summation of the numbers that contribute to the change in K, in any of the three intervals yields a positive tendency which, in fact, is greater than the one exhibited by the actual results at this time (Fig. 17). This deviation indicates that truncation and smoothing in the numerical procedure cause an extra dissipation. With regard to the above discussion of the possible uncertainty in the summation, however, the artificial dissipation may not necessarily be as large as indicated by the diagnosis shown in Fig. 19.

The numbers presented in Fig. 19 have not come out as differences between very large terms—contrary to the way tendencies appear. Thus, except for the tendencies, the numbers are quite reliable for a diagnostic examination of the energy transfers.

As a first general observation we notice that the model cyclone reveals the typical atmospheric feature of converting only a small fraction of the potential energy to kinetic energy. Furthermore, we see that the import of kinetic energy to the inner region, is as important for the maintenance of kinetic energy in that region as the production is. Farther out the conversion (P, K) is of dominant importance and occurs at such a high rate that a part of the produced kinetic energy can be transported inwards. We may state—as Ooyama (1969) did—that, regarding production and dissipation of kinetic energy, the storm is roughly self-contained inside an area of about 500 km. The mean rate of production inside this radius is in the present case (at 84^h) about 20 Watts/m^2. (This is nearly the same rate of production as estimated for extra-tropical cyclone areas; see Palmén & Newton, 1969.)

It is interesting to note the very small contribution to the budget of latent energy from the sea surface inside 200 km radius. Not until we consider a vortex with a radius of about 400–500 km does the energy flux from the sea surface play a noticeable role ($>10\%$) in the budget of the latent energy. The present results indeed emphasize the statement by Palmén & Newton (1969) that the essential energy source is derived from the lateral influx of water vapor.

Both the qualitative and the quantitative features of the budget displayed in Fig. 19 are in a reasonably good agreement with Ooyama's (1969) and Rosenthal's (1969) model results. Also do the results compare well with those obtained from budget studies of individual and mean hurricane data (e.g., Palmén & Riehl, 1957; Riehl & Malkus, 1961; Miller, 1962; Anthes & Johnson, 1968; Hawkins & Rubsam, 1968*b*; Palmén & Newton, 1969).

The flux of sensible heat from the sea surface seems small in comparison with the estimates by Malkus & Riehl (1960) and Haskins & Rubsam (1968*b*). The figure 2.9×10^{12} Watts corresponds to a mean flux of 92 Watts/m^2 within radius 100 km, while the values given in the above papers are 190 Watts/m^2 and 195 Watts/m^2 respectively. (In the author's opinion, the temperature difference between sea and air, adopted by Hawkins & Rubsam, seems however somewhat large.) The relatively small value, produced by the model, is connected with an unexpectedly small temperature difference $(T_w - T_s)$ which does not exceed 1.5°C at any time during the integration. A preliminary experiment with a finer horizontal resolution has indicated that the small difference in the present case may be due to the rather coarse grid along r.

The radial distribution of the surface stress, (τ_s), at 84^h is presented in Fig. 20, together with the distributions deduced by Palmén & Riehl (1957) and by Malkus & Riehl (1960). The discrepancy within 100 km, revealed in the figure, is essentially due to the fact that the maximum tangential wind is located closer to the centre in the model hurricane, studied by Malkus & Riehl, than in the cyclone of the present experiment. The agreement is as good as we may expect with regard to the horizontal resolution employed in the present computations.

Even without making comparisons with other results, the study of the energy budget is still of great interest, since it constitutes an important check on the internal consistency of the behaviour of the model storm. The energy bud-

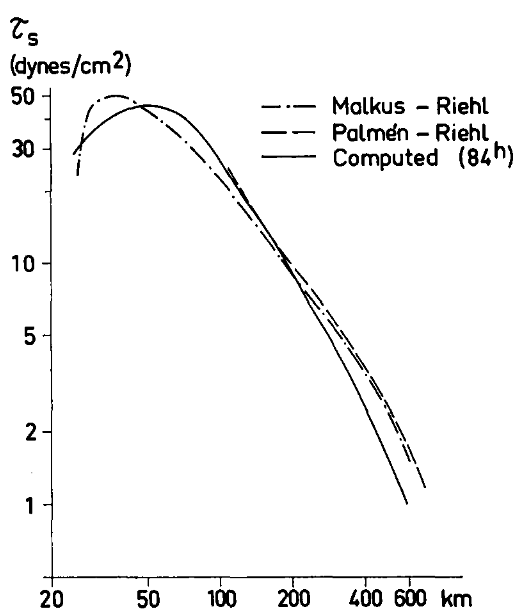

Fig. 20. Tangential component of the surface stress versus radius. Dashed line from budget studies by Palmén & Riehl (1957) for mean hurricane data; ——, from model moderate storm studied by Malkus & Riehl (1960); –·–·–, from the present model at 84^h.

get, presented in Fig. 19, demonstrates that there exists a good consistency energetically. In addition, the above comparison with other results shows that the various forms of the energy participate in the transformation processes in a realistic manner—both with regard to intensity and to radial distribution.

7. Summary

The results obtained from an integration over 210 hours show that the model is able to simulate what is considered a typical life cycle of a tropical cyclone, with a good deal of reality. It is also demonstrated that the detailed structure of the model vortex—in the vertical as well as in the horizontal—at the mature stage has a noteworthy resemblance to that of real hurricanes.

Furthermore, the results indicate that there exsists a convincing interdependent consistency during the development. The model may hence be used with confidence for various experiments, such as studies of how different external conditions affect the evolution. One may likewise get valuable information on the importance of different physical processes, by introducing new ones in the model, or by trying different plausible alternative hypotheses of the existing ones. Part of a comparison of the latter kind has been presented, where it was revealed that the rate of intensification, to a considerable degree, is determined by our formulation of how the condensational heating becomes distributed vertically in terms of the large scale variables. This fact emphasizes the need for continued and possibly intensified observational and theoretical studies on the interplay between cumulunimbi and their environment.

We have directed attention to some problems in the numerical treatment. In the very intense system, with regard to gradients and curvatures, computational disturbances, originating from the boundaries, become detectable in spite of a computationally stable boundary treatment. Consequently, an artificial damping has been introduced through a smoothing procedure. This operation may possibly have caused a somewhat enhanced decline of the physical system.

The rather coarse resolution along the radius has necessitated some caution in the discussion of the very detailed structure in the core region. Hence a comparative experiment with a much finer resolution would be of great interest. As mentioned above, however, it is also quite plausible to perform relevant comparisons using the present radial resolution, i.e., comparisons which are of a more direct, physical nature. A few such experiments will be presented in another paper (Sundqvist, 1970).

Acknowledgement

I wish to express my sincere thanks to Professor Bert Bolin and Professor Bo Döös who have offered stimulating and valuable criticisms in a number of discussions. I am also greatly indebted to Professor George Veronis, Yale University, New Haven, with whom I have had many helpful discussions when he was visiting the institute in Stockholm.

I would like to thank the Staff members of the National Hurricane Research Laboratory, Miami, for many interesting and enlightening conversations during an inspiring visit there. The visit was in part sponsored by ESSA.

APPENDIX

A.1. *The prognostic equations*

We may illustrate the typical treatment of any one of the prognostic equations by considering

$$\frac{\partial \varphi}{\partial t} = -u\frac{\partial \varphi}{\partial r} + K_H \frac{\partial^2 \varphi}{\partial r^2} + \frac{\partial}{\partial p}\left[Kv\frac{\partial \varphi}{\partial p}\right]$$

and its finite difference analogue

$$\frac{\varphi_{ij}^{\tau+1} - \varphi_{ij}^{\tau-1}}{2\Delta t} = -\frac{1}{j\Delta r}\frac{\psi_{i+1j} - \psi_{i-1j}}{2\Delta p}\cdot\frac{\varphi_{ij+1}^{\tau} - \varphi_{ij+1}^{\tau}}{2\Delta r} + \frac{K_H}{\Delta r^2}(\varphi_{ij+1}^{\tau-1} + \varphi_{ij-1}^{\tau-1} - 2\varphi_{ij}^{\tau-1}) + \frac{1}{\Delta p^2} \times [K_{i+\frac{1}{2}}(\varphi_{i+1j}^{\tau-1} - \varphi_{ij}^{\tau-1}) - K_{i-\frac{1}{2}}(\varphi_{ij}^{\tau-1} - \varphi_{i-1j}^{\tau-1})] \quad \text{(A 1.1)}$$

where φ is an arbitrary variable. To show the principle, we only consider the radial advection here; and u is rewritten according to (2.8 a). The notations are the conventional ones and it is sufficient to state:

$$\tau \cdot \Delta t = t \qquad \text{(elapsed time)}$$

$$i\Delta p = p$$

$$j\Delta r = r$$

Expression (A 1.1.) shows the evaluation of first and second order derivatives; of course the analogous expressions are used in the diagnostic equations. We note that an explicit scheme is used, which, in order to secure computational stability, limits Δt and requires advective terms to be computed at time τ and diffusion terms at $(\tau - 1)$. See, e.g., Phillips, (1960); Richtmyer & Morton, (1967).

According to a linear analysis we find the criterion on Δt for stability:

$$\Delta t < \frac{1}{\sqrt{2a^2 + 16b^2} + 4b} \qquad \text{(A 1.2)}$$

where

$$a = \frac{|\bar{u}|_{\max}}{\Delta r}$$

and

$$b = \frac{K_H}{\Delta r^2} + \frac{(K_v)_{\max}}{\Delta p^2}$$

Note that a is obtained from the boundary layer radial velocity so that no special subdivision of Δt is necessary.

As the vortex intensifies, the first term under the radical in (A 1.2) becomes dominant and the criterion approaches the classical one due to Courant-Friedrichs-Lewy.

Let us denote the right hand side of (A 1.2) by Δt_c.

The marginal increment, Δt_c, is computed each time step. If the value for Δt being used lies outside the interval $0.8 \cdot \Delta t_c - 0.9 \cdot \Delta t_c$ we put $\Delta t = 0.9 \cdot \Delta t_c$. Hence, there is not a strict centering in time; in the actual computations, however, the mean change in Δt per step, during the period when Δt goes from its largest to its smallest value, is only 0.5–1.0 %.

It also deserves mentioning that the product $(\xi \cdot \Delta t)$ remains relatively small (<0.3) throughout the period of integration. Therefore the condensational heating is not subject to any serious truncation because of large time increments.

Concerning the momentum equation, (2.11), we note the following. The relative vorticity $(\partial v/\partial r + v/r)$ is approximated by the finite difference analogue for $1/r\, \partial/\partial r\,(rv)$; i.e., angular momentum rather than momentum is forecast.

The friction due to vertical shear at 900 mb is approximated by

$$\left(\frac{\partial \tau}{\partial p}\right)_{900} = \frac{\tau_s - \tau_{800}}{2\Delta p} \qquad \text{(A 1.3)}$$

where τ_{800} is obtained from the difference $(v_{900} - v_{700})$ and the eddy viscosity given by the algebraic mean of K_v at 850 and 750 mb.

At 100 mb, the radial velocity is obtained by one-sided differencing. Since $\psi_{100} = 0$

$$u_{100} = \frac{\psi_{200}}{r\Delta p}$$

At the lateral boundaries, where *outflow* from the computational domain occurs, we cannot prescribe the boundary conditions arbitrarily; if inadequate conditions are applied, unstable computational models are created which spread inwards from the boundaries (see Platzman, 1954; and Phillips, 1960). It is important to note that this circumstance must be considered at both lateral boundaries. At the *centre*, this fact becomes masked because of the symmetry and because it is natural to assume $v = 0$ there. The boundary of the numerical analogue, however, is rather at the first internal gridpoint, and if there is a radial flow towards the centre, a treatment similar to the one at the points of outflow on the outer boundary is required. (This requirement becomes more obvious, if for instance, v is defined at 0.5 Δr, 1.5 Δr etc.) In fact, experiments with the present model have shown that a correct boundary treatment in the centre is even more important than at $r = r_{\max}$ because of the large relative vorticity in the central parts of the vortex.

In the present integrations two different methods have been employed in order to avoid the above-mentioned instabilities:

(i) a linearextrapolation according to the formula

$$\varphi_B^{\tau+1} = \varphi_{B-1}^{\tau+2} + \varphi_{B-1}^{\tau} - \varphi_{B-2}^{\tau+1} \qquad \text{(A 1.4)}$$

where B stands for boundary and $(B-1)$ and

$(B-2)$ denote the first and second points inside the boundary respectively:

(ii) up-stream differencing.

Method (i) has been proposed by A. Sundström (personal communication). It yields stability, because the sum of φ_{B-1} at times τ and $(\tau+2)$ enters; if we instead take $2\,\varphi_{B-1}^{\tau+1}$, instability is introduced as shown by Platzman (1954). Method (i) is applied in both the prognostic equations (2.11 and 2.13) at the outer boundary.

Since $\varphi_{B-1}^{\tau+2}$ is unknown, equation (A 1.4) and the prognostic equation for φ_{B-1} are solved simultaneously, using the same advective velocities as for obtaining $\varphi_{B-1}^{\tau+1}$.

Method (ii) is applied in the centre. Upstream differences are used in the vertical as well as in the horizontal and therefore the stability criterion for Δt, (A 1.1) remains the same as for the interior.

As mentioned in section 4, up-stream differences are employed for the momentum equation at all points in the first two columns inside $r=0$. This is an unnecessarily cautious treatment, since an application of method (ii) (or i) is necessary only at the first internal gridpoint where $u<0$. A comparative experiment over a limited period of integration has been performed, using one-sided differences only in the first point column. The differences in the results were negligible.

The application of the above-mentioned boundary treatment is not required for the water vapor equation at the centre, partly because of weak gradients in q, but essentially because saturation is reached in the convective region, and thus q is put equal to the saturation value for the current temperature.

There are no apparent numerical reasons for preferring one method to the other; practically, of course, method (ii) is easier to handle. Neither of the two eliminates oscillations completely, but rather suppresses them. This is certainly partly the reason why oscillations with the period $2\Delta t$ are detectable in the results from integrations when no smoothing is applied. Such fluctuations are no longer noticed when smoothing is introduced, thus stabilizing the computational scheme further.

If we denote the smooothed value of v by v^* and the angular momentum by $M_{ij}=r_j \cdot v_{ij}$, we have

$$v_{ij}^* = v_{ij} + \frac{s}{r_j}\left[M_{ij+1}+M_{ij-1}+M_{i+1j}+M_{i-1j} + \frac{1}{2j}(M_{ij+1}-M_{ij-1}) - 4M_{ij}\right] \qquad \text{(A 1.5)}$$

where $s=1/80$ in the present application.

A 2. *The diagnostic equations*

As mentioned in section 5 we assumed that the *surface pressure* (p_s) can be obtained from gradient balance using the tangential wind at 900 mb. Thus

$$\frac{\partial}{\partial r}(\log p_s) = \frac{1}{RT_s}\left(fv+\frac{v^2}{r}\right)_{900} \qquad \text{(A 2.1)}$$

where T_s is the surface temperature obtained from (5.2).

The thermal equation, (2.12), as well as equation (A 2.1) is integrated by the trapezoidal formula from $r=r_{\max}$ to $r=0$.

The quantities A through D, (2.15 a–d), in the *equation for the meridional circulation*, (2.14), are evaluated at all internal gridpoints. The absolute vorticity, $(f+\partial v/\partial r+v/r)$, in (2.15a) as well as $\partial v/\partial p$ in (2.15b) are computed in the same way as corresponding terms in the prognostic equation (2.11). The coefficient B, (2.15b) is also computed at $r=r_{\max}$ (and at $r=0$ where $B=0$), so that the third order horizontal derivative of θ in D is obtained at the points next to the lateral boundaries.

The rule for evaluation of

$$\frac{\partial}{\partial p}\left[g\left(f+\frac{2v}{r}\right)\frac{\partial\tau}{\partial p}\right]$$

in D is obvious for gridpoints from 800 mb and upwards (putting $K_v=0$ at 50 mb). At 900 mb, we expand this derivative into two terms:

$$\frac{2g}{r}\cdot\frac{\partial v}{\partial p}\cdot\frac{\partial\tau}{\partial p} + g\left(f+\frac{2v}{r}\right)\frac{\partial^2\tau}{\partial p^2}$$

The internal stresses that appear in the conventional difference analogue of this expression are approximated in the same way as τ_{800} of the momentum equation at 900 mb.

The iterative procedure for solving the finite difference analogue of the elliptic equation (2.14) requires a calculation time that is an appreciable part of the total time. It would therefore be of interest to report on some of the experimental experiences gained during the work on the model.

When employing the Liebmann relaxation method (see e.g., Thompson, 1961) it is difficult to know the optimal coefficient of relaxation because the equation (2.14) has variable coefficients. Furthermore, it has turned out that the number of iterations increases if higher resolution is used along the radius; i.e., when the ratio J/I increases, I and J being the number of gridpoints along p and r respectively.

The Liebmann method has been applied in two different ways:

(i) the grid is swept row by row, and the same procedure is repeated each iteration;
(ii) the grid is swept row by row every second iteration and every second one, column by column; This procedure was most efficient when the relaxation coefficient had slightly different values for the two directions.

Version (ii) rendered convergence for a number of iterations that was 30–40% less than was needed for version (i).

Furthermore, some experiments have been carried out (with version (ii)) in which ψ was solved only at every second point of the field at the beginning of the relaxation, in order to reduce first the large scale error field. When the maximum error was less than two to five times the final tolerance, ψ-values were assigned to all points by linear interpolation and then the relaxation was completed. The experiments showed that it did not pay off to solve too accurately for ψ on the coarse grid. In comparison with version (ii) this method reduced the number of iterations by 20–25% (and hence the execution time somewhat more) in the best cases.

Finally, an alternating-direction (ADI) method (see Richtmyer & Morton, 1967) has been employed as the iterative procedure for solving equation (2.14). This method has proved to be the most efficient one of those tried in the present computations. For the general case it is difficult to prove that this method makes ψ converge to the true solution. We shall, however, under simplifying assumptions, show that the error in ψ decreases monotonously in this iterative procedure.

In order to describe the method specifically, we shall use the following notations

$$a_{ij} = \frac{A_{ij}}{\Delta p^2}; \quad b_{ij} = \frac{B_{ij}}{\Delta r\,\Delta p}; \quad c_{ij} = \frac{C_{ij}}{\Delta r^2}$$

$$a'_{ij} = a_{ij} - \frac{2}{j} b_{ij}$$

$$a''_{ij} = a_{ij} + \frac{2}{j} b_{ij}$$

$$c'_{ij} = c_{ij} - \left[\frac{1-\varkappa}{2i} b_{ij} + \frac{c_{ij}}{2j}\right]$$

$$c''_{ij} = 2c_{ij} - c'_{ii}$$

$$e_{ij} = a_{ij} + c_{ij}$$

where A, B, C are given by (2.15a–b).

Let us furthermore denote the second term of (2.14) by $f(\psi)$.

Then the finite difference analogue of (2.14) for two successive iterations may be written (the subscripts of the coefficients are dropped since they refer to $(i;\,j)$ in all cases):

$$-a'\psi^{\nu+1}_{i+1j} + 2e\,\psi^{\nu+1}_{ij} - a''\psi^{\nu+1}_{i-1j} = -r_j D_{ij} + c'\psi^{\nu}_{ij+1} + c''\psi^{\nu}_{ij-1} + f(\psi^{\nu}) \qquad \text{(A 2.2 a)}$$

$$-c'\psi^{\nu+2}_{ij+1} + 2e\,\psi^{\nu+2}_{ij} - c''\psi^{\nu+2}_{ij-1} = -r_j D_{ij} + a'\psi^{\nu+1}_{i+1j} + a''\psi^{\nu+1}_{i-1j} + f(\psi^{\nu+1}) \qquad \text{(A 2.2 b)}$$

where ψ^{ν} is the approximation of ψ at the νth iteration. We first solve (A2.2a) exactly for each column, and then (A2.2b) for each row; thereafter we return to (A2.2a) etc., unless the maximum error is smaller than the prescribed tolerance. The term $f(\psi)$ only appears on the right hand side of the equation because of the form of the difference analogue of the mixed second order derivative of ψ.

We shall show that ψ^{ν} converges towards the true value for the barotropic case ($b = f(\psi) = 0$) and for constant a and c (or the convergence factor being a local property). Denoting the error at the νth iteration by $\varepsilon^{\nu} = \psi^{\nu} - \psi$ we thus get from (A2.2):

$$a(\varepsilon^{\nu+1}_{i+1j} + \varepsilon^{\nu+1}_{i-1j}) + 2(a+c)\,\varepsilon^{\nu+1}_{ii} + c(\varepsilon^{\nu}_{ij+1} + \varepsilon^{\nu}_{ij-1}) = 0 \qquad \text{(A 2.3 a)}$$

$$c(\varepsilon^{\nu+2}_{ij+1} + \varepsilon^{\nu+2}_{ij-1}) + 2(a+c)\,\varepsilon^{\nu+2}_{ij} + a(\varepsilon^{\nu+1}_{i+1j} + \varepsilon^{\nu+1}_{i-1j}) = 0 \qquad \text{(A 2.3 b)}$$

We assume $\varepsilon = 0$ on the boundaries and consider a Fourier component

$$\varepsilon_{ij}^{\nu} = E_{kl}^{\nu} \sin ki\Delta p \sin lj\Delta r.$$

Express the amplitude as

$$E^{\nu+1} = \lambda_1 E^{\nu}$$

and $$E^{\nu+2} = \lambda_2 E^{\nu+1} = \lambda_1 \lambda_2 E^{\nu}.$$

Thus we require $|\lambda_1| < 1$ and $|\lambda_2| < 1$—or at least $|\lambda_1 \lambda_2| < 1$—for convergence.

Utilizing trigonometric relations we solve for λ_1 and λ_2 in (A 2.3 a) and (A 2.3 b) respectively and find

$$\lambda_1 \cdot \lambda_2 = \frac{ac \cdot \cos k\Delta p \cos l\Delta r}{[c + a(1 - \cos k\Delta p)]\,[a + c(1 - \cos l\Delta r)]}$$

Provided $a > 0$ and $c > 0$—as we have assumed in section 2.2—we easily establish that $|\lambda_1 \lambda_2|$ would have a maximum for
$\cos k\Delta p = 1$ and $\cos l\Delta r = 1$. Hence $|\lambda_1 \lambda_2| < 1$.

If we solve for the two λ individually we notice that, because $c/a \gg 1$, the damping by λ_2 becomes considerably more efficient than by λ_1. Furthermore we notice that the method even yields convergence for a Poisson or Helmholtz equation; in these cases, however, $a = c = 1$ (square meshes), and the convergence would not be as rapid as in the present application.

The tridiagonal systems, (A2.2a and b), having positive coefficients are solved by Gauss' elimination method (Richtmyer & Morton, 1967).

Parallel integrations over 24 and 48 hours have been peformed using Liebmann relaxation (the above version (ii)) and the ADI method. Within the accuracy with which the print-outs are given, the results do not differ.

Comparative experiments with different resolution along the radius have also been carried out. The Liebmann method showed a strong increase in the number of iterations as the resolution was increased, while the ADI method showed a much more moderate increase. If we denote the average number of iterations per time step by $N_L(n)$ and $N_{AD}(n)$ for respective procedure, the differences may be illustrated by the following ratios; n is the number of points along r (along p it is 10)

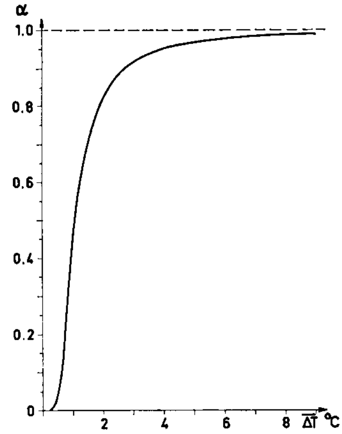

Fig. A1. The function $\alpha\,(\overline{\Delta T})$ that gives the transition from phase (ii) to phase (iii) in the condensation processes (section 3.1); $\gamma = 0.8$.

$$(a)\ \frac{N_L(41)}{N_L(21)} \simeq 4; \qquad (b)\ \frac{N_{AD}(41)}{N_{AD}(21)} \simeq 1.3;$$

$$(c)\ \frac{N_L(41)}{N_{AD}(41)} \simeq 3.3 \qquad (d)\ \frac{N_L(21)}{N_{AD}(21)} \simeq 1.1;$$

The ratios (a) and (c) can probably be reduced by searching for a more efficient relaxation coefficient for $n = 41$. This difficult task is avoided however, by employing the ADI method.

A 3. *The condensational heating*

The numerical procedures in connection with the computation of the condensational heating, Q, are straightforward and only a few remarks are considered necessary in this context.

To describe the specific computation of T_c and q_c along a pseudo-adiabat (θ_E = const.), let us assume that we have obtained T_c, q_c at a level p_1 and thus the slope $\Gamma_s(T_c, q_c, p_1)$ of the adiabat there. Integration to the next level $p_2 = p_1 - \Delta p$ is performed with the trapezoidal formula using the slope $\Gamma_s(T, q, p_2)$ according to the environmental temperature and humidity at p_2. The approximate temperature $T_c^*(p_2)$ thus obtained gives, together with θ_E, a value for $q_c^*(p_2)$ that makes θ_E = constant. Consequently, if T_c has become too small, q_c will be too large and vice versa. Therefore a final correction according to a generalized wet-bulb procedure is performed:

$$T_c = T_c^* - \frac{L}{c_p}(q_c - q_c^*)$$

where, with sufficient accuracy

$$q_c = q_s(T_c) = q_s(T_c^*)\left[1 + \frac{\varepsilon L}{RT_c^{*2}}(T_c - T_c^*)\right];$$

subscript "s" stands for saturation and $\varepsilon = 0.622$.

The T_c-value obtained in this way is generally a slight underestimate of the true T_c-value; the maximum deviation, which occurs at high altitudes, is however, less than 1°C. The q_c-value has of course the corresponding accuracy.

The continuous transition from phase (ii) to phase (iii) (section 3.1) is expressed in the following manner

$$Q = \alpha Q_1 + (1-\alpha) Q_2$$

where Q_1 and Q_2 are the heating rates according to expressions (3.1) and (3.6) respectively;

$$\alpha = e^{-\beta}; \quad \beta = \left(\frac{\gamma}{\overline{\Delta T}}\right)^2$$

where γ is a constant and $\overline{\Delta T}$ is the mean temperature difference $(T_c - T)$ in the penetrated layer, i.e.

$$\overline{\Delta T} = \frac{1}{p_B - p_T}\int_{p_T}^{p_B} (T_c - T)\, dp$$

In the present computations $\gamma = 0.8$. Fig. A 1 shows the function α for this value of γ. We see for instanae that $\alpha = 0.97$ for $\overline{\Delta T} = 5$°C and $\alpha = 0.75$ for $\overline{\Delta T} = 1.5$°C and when $\overline{\Delta T} = 0.5$°C then $\alpha = 0.077$. The typical range for $\overline{\Delta T}$ during the intensification is 5–10°C. In the stage of maximum intensity $\overline{\Delta T} \simeq 1$°C near the centre.

REFERENCES

Alaka, M. A. 1963. Instability aspects of hurricane genesis. *Nat. Hurricane Res. Proj. Report 64*

Anthes, R. A. & Johnson, D. R. 1967. The generation of available potential energy in hurricane Hilda (1964). Men. Wea. Rev., 96, 291–302.

Charney, J. G. & Eliassen, A. 1964. On the growth of the hurricane depression. *J. Atm. Sci. 21*, 68–75.

Colon, J. A. & Staff 1961. On the structure of hurricane Daisy 1958. *Nat. Hurricane Res. Proj. Report 48.*

Dunn, G. E. & Miller, B. I. 1964. *Atlantic Hurricanes.* Louisiana State University Press, Baton Rouge.

Eliassen, A. 1952. Slow thermally or frictionally controlled meridional circulation in a circular vortex. *Astrophysica Norvegica 2*, 19–60.

Gray, W. M. 1966. On the scales of motion and internal stress characteristics of the hurricane. *J. Atm. Sci. 23*, 278–288.

Haque, S. M. A. 1952. The initiation of cyclonic circulation in a vertically unstable stagnant air mass. *Quart. J. R. meteor. Soc. 78.*

Hawkins, H. F. & Rubsam, D. T. 1968*a*. Hurricane Hilda 1964: I. Genesis, as revealed by satellite photographs, conventional and aircraft data. *Mon. Wea. Rev. 96*, 428–452.

— 1968*b*. Hurricane Hilda 1964: II. Structure and budgets of the hurricane on October 1, 1964. *Mon. Wea. Rev. 96*, 617–636.

Jordan, C. L. 1958. Mean soundings for the West Indies area. *J. Meteor. 15*, 91–97.

Kasahara, A. 1961. A numerical experiment on the development of a tropical cyclone. *J. Meteor. 18*, 259–282.

Kleinschmidt, E. 1951. Grundlagen einer Theorie der tropischen Zyklonen. *Arch. Meteor. Geophys. Bioklimat. A 4*, 53–72.

Kuo, H. L. 1961 Convection in conditionally unstable atmosphere. *Tellus 13*, 441–459.

— 1965. On the formation and intensification of tropical cyclones through latent hear release by cumulus convection. *J. Atm. Sci. 22*, 40–63.

Lilly, D. K. 1960. On the theory of disturbances in a conditionally unstable atmosphere. *Mon. Wea. Rev. 88*, 1–17.

Malkus, J. S & Riehl, H. 1960. On the dynamics and energy transformations in steady state hurricanes. *Tellus 12*, 1–20.

Miller, B. I. 1962. On the momentum and energy balance of hurricane Helene (1958). *Nat. Hurricane Res. Proj. Report 53.*

— 1963. On the filling of tropical cyclones over land. *Nat. Hurricane Res. Proj. Report 66.*

Ogura, Y. 1964. Frictionally controlled, thermally driven circulation in a circular vortex with application to tropical cyclones. *J. Atm. Sci. 21*, 610–621.

Ooyama, K. 1964. A dynamical model for the study of tropical cyclone development. *Geofisica Internacional 4*, 187–198.

— 1966. On the stability of the baroclinic circular vortex: a sufficient criterion for instability. *J. Atm. Sci. 23*, 43–53.

— 1969. Numerical simulation of the life cycle of tropical cyclones. *J. Atm. Sci. 26*, 3–40. (First published in *Geophysical Sci. Lab. Report No. TR 67-9*, 1967, New York University.)

— 1969*a*. Numerical simulation of tropial cyclones with an axi-symmetric model. *Proceedings of the WMO/IUGG Symposium on Numerical Weather Prediction in Tokyo, 1968, pp. III: 81–88.* Japan Meteor. Agency, 1969.

Palmén, E. & Newton, C. W. 1969. *Atmospheric circulation systems.* International Geophysics series Vol. 13. Academic Press, New York and London, pp. 471–560.

Palmén, E. & Riehl, H. 1957. Budget of angular momentum and energy in tropical cyclones. *J. Meteor. 14*, 150–159.

Phillips, N. A. 1960. Numerical weather prediction. In *Advances in computers (ed. F. C. Alt), Vol. 1*, 43–90.

Platzman, G. W. 1954. The computational stability of boundary conditions in numerical integration of the vorticity equation. *Arch. Met., Wien A 7*, 29–40.

Richtmyer, R. D. & Morton, K. W. 1967. *Difference methods for initial value problems*. Interscience Publishers, New York.

Riehl, H. & Malkus, J. S. 1961. Some aspects of hurricane Daisy, 1958. *Tellus 13*, 181–213.

Rosenthal, S. L. 1964. Some attempts to simulate the development of tropical cyclones by numerical methods. *Mon. Wea. Rev. 92*, 1–21.

— 1969. Numerical experiments with a multilevel primitive equation model designed to stimulate the development of tropical cyclones. Experiment I. *ESSA Tech. Memo. ERLTM-NHRL 82*. 36 pp.

Sawyer, J. S. 1947. Notes on the theory of tropical cyclones. *Quart. J. R. Met. Soc. 73*, 101–126.

Sheppard, P. A. 1958. Transfer across the earth's surface and through the air above. *Quart. J. R. Met. Soc. 84*, 205–224.

Sundqvist, H. 1970. Numerical simulation of the development of tropical cyclones with a ten-level model. Part II. *Tellus 22*, (To be published).

Sundqvist, H. & Veronis, G. 1970. A simple finite-difference grid with non-constant intervals. *Tellus 22*, 26–31.

Syono, S. 1953. On the formation of tropical cyclones. *Tellus 5*, 179–195.

— 1962. A numerical experiment of the formation of tropical cyclones. *Proc. Intern. Symposium on Numerical Weather Prediction, Tokyo, 1960*, pp. 405–418. Meteor. Soc. of Japan, 1962.

Syono, S. & Yamasaki, M. 1966. Stability of symmetrical motions driven by latent heat release by cumulus convection under the existence of surface friction. *J. Met. Soc. Japan 44*, 353–375.

Thompson, P. D. 1961. *Numerical weather prediction*. Macmillan, New York.

Wallington, C. E. 1962. The use of smoothing or filtering operators in numerical forecasting. *Quart. J. R. Met. Soc. 88*, 470–484.

Wu, J. 1969. Wind stress and surface roughness at air–sea interface. *J. Geophys. Res. 74*, 444–455.

Yamasaki, M. 1968*a*. Numerical simulation of tropical cyclone development with the use of primitive equations. *J. Met. Soc. Japan 46*, 178–201.

— 1968*b*. A tropical cyclone model with parameterized vertical partition of released latent heat. *J. Met. Soc. Japan 46*, 202–214.

Yanai, M. 1961*a*. A detailed analysis of typhoon formation. *J. Met. Soc. Japan 39*, 187–214.

— 1961*b*. Dynamical aspects of typhoon formation. *J. Met. Soc. Japan 39*, 282–309.

— 1964. Formation of tropical cyclones. *Rev. Geophysics 2*, 367–414.

Zipser, E. J. 1964. On the thermal structure of developing tropical cyclones. *Nat. Hurricane Res. Proj. Report 67*.

ЧИСЛЕННОЕ МОДЕЛИРОВАНИЕ ЭВОЛЮЦИИ ТРОПИЧЕСКИХ ЦИКЛОНОВ С ПОМОЩЬЮ ДЕСЯТИУРОВЕННОЙ МОДЕЛИ: ЧАСТЬ

Построена динамическая модель ассиметричного вихря при условии квазибаланса. Эффект конвекции включен в модель путем параметризации; проинтегрированное по вертикали выделение тепла определяется по конвергенции водяного пара на нижнем уровне.

Модель вертикального распределения выделения скрытого тепла основана на интуитивных соображениях, так как нет достаточных сведений о реальном механизме этого выделения с помощью кучево-дождевых облаков. Качественное обсуждение вопроса приводит нас к априорному механизму явления, зависящему от различных возможных функциональных форм, описывающих нагревание по вертикали. Сравниваются два численных експеримента с различным вертикальным распределением нагрева и обнаруживается существенная разница в скорости интенсификации.

Детально показаны результаты эксперимента, по которым можно судить о наиболее реалистических значениях скорости интенсификации. Сравнение с эмпирическими данными о тропических циклонах указывает на то, что модель довольно хорошо моделирует природу. Диагностическое изучение энергетического баланса тропического циклона показывает, что модель энергетически достаточно хорошо согласована. Скорости преобразования различных типов энергии в системе вполне сравнимы с соответствующими эмпирическими значениями.